Simulating the Behaviour of Reactive Soils and Slab Foundations using Hydro-Mechanical Finite Element Modelling Incorporating Soil Suction and Moisture Changes

Mohamed A. Shams

PhD Candidate, Department of Civil Engineering, Curtin University, WA 6845, Australia

E-mail: mohamed.shams@postgrad.curtin.edu.au

Mohamed A. Shahin†

Associate Professor, Department of Civil Engineering, Curtin University, WA 6845, Australia

E-mail: M.Shahin@curtin.edu.au

Mostafa A. Ismail

Geotechnical Engineering Consultant, Perth WA, Australia

E-mail: mostafaperth@gmail.com

†Corresponding author

Submitted to: **Computers and Geotechnics**

Simulating the Behaviour of Reactive Soils and Slab Foundations using Hydro-Mechanical Finite Element Modelling Incorporating Soil Suction and Moisture Changes

Mohamed A. Shams, Mohamed A. Shahin and Mostafa A. Ismail

Abstract

The main objective of this paper is to enhance the current design practice of stiffened slab foundations on reactive soils through an advanced numerical modelling study. The paper presents sophisticated three-dimensional (3D) hydro-mechanical finite element (FE) numerical models using coupled flow-deformation and stress analyses capable of simulating the complex behaviour of reactive soils and slab foundations. The decisive parameters of the developed FE models are described in detail and the modelling efficacy is verified through three case studies. The ability of the FE models to simulate the moisture diffusion and suction variations in relation to climate changes is validated through two case studies involving field observations. A third case study involving a hypothetical stiffened slab foundation on reactive soil is used for comparison with one of the traditional design methods. The developed FE models are found to perform well and overcome some of the most significant limitations of available traditional methods, leading to more reliable design outputs.

Keywords: Slab foundations, Reactive soils, Lightweight structures, Hydro-mechanical numerical modelling, Finite element method.

1. Introduction

Reactive (expansive) soils swell and shrink by increase and decrease of soil moisture between the wet and dry seasons, causing lightweight structures to suffer from different levels of structural damages due to foundation movements. The financial losses incurred due to damages caused to structures built on reactive soils are alarming; it has been estimated to be US$7 billion per year [1]. It was also reported that the annual losses in the United States could reach up to US$11 billion for houses and roads damaged by swelling of reactive soils [2]. The American Society of Civil Engineers estimated that nearly 25% of all homes in the United States suffered some damage due to reactive soils, with the financial losses exceeding those caused by natural disasters such as earthquakes, floods, hurricanes and tornadoes combined [3]. Similarly, reactive soils cover roughly 20% of Australia and cause structural cracks to nearly 50,000 houses each year, forming about 80% of all housing insurance claims [4].

Over the last 50 years or so, stiffened slab foundations have been used as a suitable foundation system for lightweight structures on reactive soils and have demonstrated historical success, despite the inherent shortcomings. The main premise underlying the design of stiffened slab foundations is to adopt idealised typical patterns of the slab foundation movements caused by soil heaves (edge or centre), assuming that these two heave scenarios (i.e. edge or centre) represent the worst loading cases among an infinite number of heave patterns, depending on the site boundary conditions. According to the extreme edge heave scenario, the stiffened slab foundation acts as a simple beam supported by the rising soil at the edges, assuming that the centre of the footing slab loses its contact with the soil. Conversely, in the centre heave scenario, the stiffened slab foundation acts as a double cantilever supported by the rising soil at the centre area while the edges of the slab lose their contact with the soil over a certain edge distance. Analysing the footing slabs over the distorted soil mounds enables the designers to obtain iteratively the required stiffness and the corresponding internal forces that maintain the foundation differential movements within certain acceptable limits. Many traditional design methods are available in the literature for the design of stiffened slab foundations on reactive soils, including the Building Research Advisory Board (BRAB) method [5], Lytton method [6], Walsh method [7], Mitchell method [8], Swinburne method [9], Post Tensioning Institute (PTI) method [10] and Wire Reinforcement Institute (WRI) method [11, 12]. Out of these methods, Walsh method [7] and Mitchell method [8] are adopted by the Australian Standard AS2870 [13].

During the last few decades, several attempts have been made to enhance the well-established traditional methods by implementing numerical modelling techniques (i.e. finite element and finite difference). For example, Fraser and Wardle [14] carried out finite element analysis for stiffened rafts on a semi-infinite elastic soil, and the footing was analysed iteratively on a pre-formed soil mound based on Walsh method. Poulos [15] used the mound shapes proposed by Lytton method in the analysis of strip footings using the finite element method in which the soil was modelled as an isotropic, homogeneous elastic half-space. Sinha and Poulos [16] carried out a study using the finite element method and analysed slab foundations on the soil mound represented by the equations proposed by Lytton method. Li [17] adopted a coupled thermo-mechanical analogy and introduced this approach as an acceptable and relatively accurate methodology for simulating the moisture diffusion and soil shrink-swell movement in reactive soils. El-Garhy and Wray [18] and Wray et al. [19] used an uncoupled approach to model the suction distribution and the corresponding volume change and surface movement of expansive soils using the finite difference technique. Fredlund et al. [20] carried out a finite element analysis in an iterative, uncoupled procedure (that is difficult to utilise for routine design) to evaluate the separation distance under the footing edge in the case of the edge drop scenario. Abdelmalak [21] and Magbo [22] modified Mitchell's diffusion equation [8] to derive a more representative solution for the suction distribution under cover and estimated a more realistic distorted soil mound that was utilised as a predefined soil mound under a flat foundation in a finite element analysis. Dafalla et al. [23] proposed a simplified design concept for a rigid substructure foundation in the form of an inverted-T of a two-storey concrete frame structure on expansive soils, and the edge heave scenario was simulated, while the centre heave scenario was omitted from the analysis. Zhang et al. [24] carried out a coupled finite element transient analysis for isolated footings on expansive soils by adopting the thermal analogy, and the work focused on the prediction of soil movement due to the evapotranspiration of grass roots and crops, involving specific vegetation data, which in most cases would not be available to geotechnical engineers.

Careful review of existing design methods and other studies on stiffened slab foundations on reactive soils revealed that a major assumption adopted by almost all methods involves simplifying the real, complex 3D moisture flow into a 2D problem, resulting in deformation incompatibility between the soil mound and supported footing. In addition, most existing methods use uncoupled approaches in which the footing is designed for stress analysis using pre-defined soil mound shapes obtained from a separate seepage analysis, with no consideration to the effect of slab loading on the formation of the soil mounds. Moreover, prediction of the soil mound shapes is determined using simple empirical equations, based on the best fit of minimal field observations. However, in reality, there is an infinite number of soil mound shapes depending on many factors, including soil suction, degree of saturation, permeability, site drainage conditions and irrigation/plantation events.

In this paper, an advanced 3D finite element (FE) numerical modelling is pursued to simulate the complex behaviour of stiffened slab foundations, which otherwise could not be realistically captured by the currently available design methods. Through a hydro-mechanical approach, the resulting FE modelling is capable of simulating the true performance of stiffened slab foundations on reactive soils, by: (1) involving a coupled flow-deformation analysis based on realistic moisture flow and suction evolution; and (2) inducing a realistic formation of the soil mound beneath the footing. The paper presents and discusses some important modelling aspects relating to unsaturated soils and the corresponding associated parameters. Development of the adopted FE numerical models is then explained and verified through three case studies.

2. Modelling aspects for unsaturated soils

2.1 Coupled versus uncoupled analyses

Design of stiffened slab foundations on reactive soils is typically a moisture transient, unsaturated soil problem [20]. Most studies carried out on this topic adopt uncoupled approaches in which the problem is solved via two phases, as follows. The first phase comprises an independent transient seepage analysis to obtain the distribution of the degree of saturation and/or the soil suction within the soil mass, for a certain time increment. The soil movement is then estimated using one of the available theories. A detailed description of the methods of estimating the soil movement can be found elsewhere [25]. By estimating the soil movement, the soil distorted mounds can be determined. In the second phase, a separate stress-deformation analysis is carried out for the soil structure interaction, by analysing the footing slab using pre-calculated distorted soil mounds obtained from the first phase. Although this approach is acceptable, the accuracy of results depends on the size of the selected time increment. In addition, the soil distorted mounds and the corresponding maximum differential movement are greatly affected by the stresses induced by the loaded footing, which is not considered in the seepage phase. Moreover, the soil properties in the stress phase is most often assumed to be constant; however, unsaturated soil properties are highly dependent on the moisture variation and the ensuing suction changes. Additionally, unlike the fully coupled flow-deformation analysis, the excess pore water pressure due to the load application in the uncoupled approach cannot be simulated [24]. Formation of the soil distorted mounds underneath the slab foundation in the coupled approach is thus correctly influenced by the combined effect of the suction evolution and the stresses induced by the footing loading. The abovementioned limitations indicate clearly that the uncoupled analysis oversimplifies the real situation compared with the coupled approach, and can thus inevitably lead to inaccurate design. To circumvent these limitations, this paper adopts a robust, fully coupled flow-deformation transient analysis for simulating the problem of stiffened slab foundations on reactive soils.

2.2 Mechanism of soil volume change

Fredlund et al. [26] described the volume change constitutive relations of unsaturated soils for a linear, elastic, isotropic material, as follows:

$$\varepsilon_x = \frac{(\sigma_x - u_w)}{E_1} - \frac{\mu_1}{E_1}(\sigma_y + \sigma_z - 2u_w) + \frac{(u_a - u_w)}{H_1} \tag{1}$$

where;

ε_x = normal strain in the x-direction;

E_1 = elastic modulus with respect to the change in effective stress $(\sigma - u_w)$;

μ_1 = Poisson's ratio with respect to the relative strains in *x*, *y* and *z* directions;

H_1 = elastic modulus with respect to the change in soil suction $(u_a - u_w)$;

σ = total normal stress;

u_a = air pressure; and

u_w = water pressure.

Similar equations can be written in the *y*- and *z*-directions. The soil volumetric strain is equal to the sum of the normal strain components, calculated as follows:

$$\varepsilon_v = C_t.\partial(\sigma - u_w) + C_a \partial(u_a - u_w) \tag{2}$$

where;

C_t = soil compressibility with respect to the change in the effective stresses; and

C_a = soil compressibility with respect to the change in the soil suction.

Equation 2 shows that the volume change in unsaturated soils is induced by the soil compressibility due to the change in the net stress caused by both the loading and suction variation. Because the suction variation within the soil mass results in volume change, it can thus be simulated mechanically in the FE modelling as compressive stresses. Many researchers assume that the air pressure is constant during the flow-deformation analysis [e.g. 24, 27, 28], and the same approach is adopted in the current study.

It should be noted that most available FE studies on the topic of simulating the volume change of expansive soils are based only on the suction and stress variations [e.g. 17, 19, 24, 29], with no consideration to the soil mineralogy. However, the soil minerals should be included as well; for example, clayey soils without highly swelling minerals in the form of montmorillonite are of no danger when exposed to high suction variation. This is evident from the volumetric shrinkage strain tests performed by Puppala et al. [30] on clay samples from Texas; these tests showed that clay samples with high content of montmorillonite had a volumetric shrinkage strains as twice as those of low content of montmorillonite. Only few studies account for the effect of minerals on the volume change of reactive soils, with the main focus being on the suction variation and not on the compressibility per se. However, a recent study carried out by Pulat et al. [31] suggests that suction is independent of soil mineralogy and cannot be used accurately to predict the volume change of reactive soils.

To account for the effect of soil suction and mineralogy on the volume change of expansive soils, sorption and moisture-swell models are introduced in the FE analyses of the current study for describing the volumetric strain with respect to the degree of saturation. The sorption model is represented by the soil-water characteristic curve (SWCC), which simulates the suction changes within the soil matrix with respect to the change in the degree of saturation [32]. The moisture-swell model, on the other hand, defines the volumetric swelling/saturation dependency of the soil matrix during the partially saturated flow condition and requires volumetric strain data with respect to the changes in the degree of saturation. The SWCC and moisture-swell models are discussed in detail below.

2.3 Parameters affecting coupled flow-deformation analysis

2.3.1 Soil-water characteristic curve (SWCC)

The soil water characteristic curve (SWCC) is one of the primary soil properties required for the transient seepage analysis in unsaturated soils. As mentioned above, the SWCC defines the suction-saturation dependency within the soil matrix. The soil suction may be matric or total. The matric suction is the capillary pressure of soil [i.e. U_a -U_w; where (U_a) is the pore-air pressure and (U_w) is the pore-water pressure]. The total suction is the sum of the matric suction and osmotic suction. At high suction values > 1500 kPa, the total suction equates the matric suction [33]. Numerous empirical equations have been proposed in the literature to generate different forms of SWCC based on laboratory test results. The following equation suggested by Fredlund et al. [33] is an example:

$$\theta = \theta_s \left[\frac{1}{\ln\left[e + (\psi / a)^n\right]} \right]^m \tag{3}$$

where;

θ = volumetric water content;

θ_s = saturated volumetric water content;

ψ = soil suction; and

a, m and n = fitting empirical parameters.

Fredlund et al. [33] reported that the parameter (a) determines the air entry value, whereas the parameters (m) and (n) control the slope of the curve (i.e. degree of soil diffusion). In this research, the SWCC is essential for the hydro-mechanical model used in the FE analyses. A representative, idealised SWCC is thus proposed (called herein ISWCC) to describe the saturation-suction relationship of unsaturated swelling clays, and the following section describes the way the ISWCC is constructed. Based on field suction data taken from the north-east of Adelaide, South Australia, Li [17] found that the surface suction could be assumed to vary in a sinusoidal manner in response to the climate cycles, as follows:

$$u(0,t) = 4.0 + \cos(2\pi\, n\, t) \tag{4}$$

where;

u = surface suction in pico-Farad (pF);

n = climate frequency (cycle/year); and

t = time variable (in months).

Equation 4 indicates that the ISWCC should cover the range of the expected suction values between 5.0 to 3.0 pF, which are equivalent to 10,000 and 100 kPa for the dry and wet conditions, respectively. Therefore, based on these limits, the fitting parameters (a) and (m) are fixed to 1000 and 1.25, respectively, to produce an ISWCC covering the required suction seasonal fluctuation range. In fact, the soil aggregation (structure) and initial moisture have no influence on the SWCC in the high ranges of suction > 20,000 kPa [34]. Moreover, the suction values < 100 kPa are considered negligible. For soil surfaces exposed directly to water, Mitchell [35] suggested that the suction value should be 2.75 pF. The fitting parameter (n) determines the slope of the curve as previously described and a value of 1.0 is chosen for it. Therefore, the fitting parameters (a), (m) and (n) are chosen to be 1000, 1.25 and 1.0, respectively. These values are chosen so that the ISWCC produces the least expected suction of 100 kPa at a reasonably high degree of saturation of about 95% and also the maximum expected suction of 10,000 kPa at a respectively low degree of saturation of about 30%. The proposed ISWCC is compared with field data obtained from different sites, and the comparison is shown in Fig. 1.

Fig. 1

It can be seen from Fig. 1 that the proposed ISWCC reasonably predicts the relationship between the degree of saturation and suction for many swelling soils obtained from different sites. Consequently, in case where no field data are available to construct the SWCC curves, the ISWCC shown in Fig. 1 can be used with reasonable accuracy. It should be noted that in the course of estimating the characteristic surface heave (y_s), the Australian Standard AS2870 [13, 36] does not recommend using a definitive SWCC, but rather proposes design values of suction changes (maximum of 1.2 pF). However, Mitchell [37] recommends higher values of up to 1.8 pF for the suction change in arid regions.

2.3.2 Moisture-swell model

The moisture-swell model relates the volumetric swelling of porous soil materials to the degree of saturation of the wetting liquid in the partially saturated flow condition. A partially saturated condition is postulated when the pore liquid pressure is negative. A typical example of a moisture-swell model is represented by Equation 5, in which the moisture-swell strain (ε_{ii}^{ms}) in any single direction can be calculated with reference to the initial saturation, as follows [38]:

$$\varepsilon_{ii}^{ms} = r_{ii}\frac{1}{3}\left(\varepsilon^{ms}(s) - \varepsilon^{ms}(s^{I})\right) \qquad (5)$$

where;

$\varepsilon^{ms}(s)$ = volumetric swelling strain at the current saturation;

$\varepsilon^{ms}(s^{I})$ = volumetric swelling strain at the initial saturation; and

r_{ii} = represents the ratios (r_{11}), (r_{22}) and (r_{33}), allowing for anisotropic swelling.

A few moisture-swell curves are found in the literature. Tripathy et al. [39] carried out a study on cyclic swelling and shrinkage paths for compacted expansive soil specimens and the results show the following features:

- The swelling and shrinkage path is reversible once the specimen reaches an equilibrium condition where the vertical deformation during swelling and shrinkage are equal. This generally occurred after about four swell–shrink cycles;
- The swell–shrink path represents a curve of an S-shape (i.e. three phases) for soil specimens subjected to cycles of swelling and full shrinkage. For specimens subjected to cycles of full swelling and partial shrinkage, the path comprises only two phases (i.e. curvilinear phase and linear normal phase); and

- Almost 80% of the total volumetric strain occurred in the linear portion of the S-shape curve. The linear portion is found within a degree of saturation that ranges between 50–80%.

Kodikara and Choi [40] showed that the relationship between the volumetric shrinkage or swell strain ($\varepsilon_{vol,swell/shrink}$) and reduction in compaction moisture content (Δw) observed during shrinkage tests follow a linear correlation that is valid for slurry and compacted clayey specimens. This relationship can be expressed as follows [40]:

$$\varepsilon_{vol,swell/shrink} = \alpha.\Delta w \quad (6)$$

where; (α) is the volumetric swell/shrinkage coefficient. The values of (α) are reported to be equal to 0.7 in the case of swelling and 0.66 in the case of shrinkage. In terms of the degree of saturation for highly plastic clays, these values are 0.26 and 0.24, respectively. The results obtained by Tripathy et al. [39] show a value of (α) of about 0.4, for both the swell and shrinkage volumetric strains in terms of the degree of saturation. On the other hand, Al-Shamrani and Dhowian [41] show that (α) = 0.18 from the triaxial compression test, which corresponds to a value of 0.5 for the oedometer test. In the current research, the volumetric swell/shrink coefficient (α) = 0.15 is used. This value is close to the value reported by Al-Shamrani and Dhowian [41] for the linear section of the moisture swell curve.

Chen [42] reported that very dry clays having a moisture content less than 15% can absorb moisture of as high as 35%, resulting in swelling that causes damage to structures. On the other hand, clays having moisture content of more than 30% indicates that most of the swelling has already taken place. Thakur et al. [43] carried out volumetric strain oedometer tests on montmorillonite and bentonite mineral samples with different compaction water contents and the results showed that the maximum potential volumetric strain was about 25%. Al-Shamrani and Dhowian [41] showed that field measurements of surface heave are best predicted by data obtained from the triaxial compression test and reported that the actual surface heave is about 1/3 of that obtained from the traditional oedometer test. Therefore, the maximum volumetric strain considered in the present research is taken as 8%, which is equivalent to one third of the maximum free swell value obtained by Thakur et al. [43] .

By integrating all of the above boundaries, an idealised moisture-swell curve (IMSC) can be constructed, in which the full swelling takes place at a water content of 30%, following an *S*-shape curve as obtained by Tripathy et al. [39]. For a highly plastic clays with porosity ranging from 0.4-0.6, the degree of saturation corresponding to 30% moisture content would be about 90%. Therefore, the moisture-swell function can be constructed to satisfy 100% swelling at about 90% degree of saturation. The slope of the linear portion of the S-shape curve can be considered to be 0.15, as described earlier, and the maximum volumetric swell strain can be limited to 8%. The developed idealised moisture-swell curve (IMSC) is shown in Fig. 2, compared to that of the Soko-Ngawi region clay, and a good agreement is obtained.

Fig. 2

It should be noted that in Fig. 2, the original data of the volumetric strain for the Soko-Ngawi clay (measured using odemeter tests) are divided by 3.0 to account for the equivalent triaxial test data, as recommended by Al-Shamrani and Dhowian [41]. It should also be noted that the IMSC shown in Fig. 2 is representative of unsaturated clays with high content of montmorillonite. Other moisture-swell curves can be constructed for clays having less montmorillonite minerals in the same manner but with different values of the maximum expected volumetric strains to be used for better surface heave simulation. Therefore, in order to predict the surface heave for any site, a moisture-swell curve for this specific site should be constructed.

2.3.3 Soil permeability and flow duration

Soil permeability is an important parameter in the calculation of seepage and in turn the formation of the soil distorted surface (i.e. the soil mound). In the coupled flow-deformation analysis, the partial differential equation governing the seepage follow into unsaturated soils is calculated as follows [44]:

$$\frac{\partial}{\partial x}\left(k_x \frac{\partial h}{\partial x}\right)+\frac{\partial}{\partial y}\left(k_y \frac{\partial h}{\partial y}\right)=m_w^2\,\gamma_w \frac{\partial h}{\partial t} \qquad (7)$$

where;

h = total pressure head,

k_x = soil permeability in the *x*-direction;

k_y = soil permeability in the *y*-direction;

γ_w = unit weight of water; and

m_w^2 = slope of the soil-water characteristic curve (SWCC).

Unlike the constant permeability premise used in saturated soils, the permeability of unsaturated soils shown in Equation 7 is not constant but dependant on the degree of saturation or soil suction [45, 46]. According to Forchheimer [47], the permeability of unsaturated soils is dependent on the fluid flow velocity, and it can be calculated as follows:

$$k_u = k_s\;k = \left(\frac{q\,\gamma_w}{[(\partial u/\partial x)-\rho\,g]}\right) \qquad (8)$$

where;

k_u = permeability of unsaturated soils;

k = permeability of fully saturated soils;

k_s = dependence factor of permeability on the saturation;

q = volumetric flow rate of the wetting liquid per unit area of soil;

γ_w = unit weight of the wetting liquid;

$\partial u / \partial x$ = change in pore water pressure with the unit length in x-direction;

ρ = density of fluid; and

g = magnitude of gravitational acceleration.

At a low flow velocity, as in the case of unsaturated soils, the term (ρg) in Equation 8 (known as the Forchheimer's term) approaches zero, and thus the permeability function is reduced to:

$$k_u = k_s\, k = \left(\frac{q\, \gamma_w}{(\partial u / \partial x)} \right) \tag{9}$$

Mitchell et al. [48] proposed that the dependence factor of the permeability (k_s) on the degree of saturation (S) can be calculated as follows:

$$k_s = S^3 \tag{10}$$

2.3.4 Stiffness of soil mound

The stiffness of the soil mound influences the soil-structure interaction between the soil and footing at the contact surface. The lower the soil mound stiffness (i.e. higher compressibility) the more ability of the footing to punch through the soil, and vice versa. The most frequently used soil-structure interaction model that represents the soil mound stiffness is the Winkler foundation model. However, this model has a major shortcoming, as it accounts only for the normal stiffness of the soil (i.e. in the form of vertical springs), with no consideration to the lateral friction between the soil and footing, which is inevitably mobilised. Another problem associated with this model is that the springs support both compression and tensile stresses, which does not allow for the expected separation that must occur between the soil and the footing under tension (as in the case of the slab foundations on expansive soils under different edge movement scenarios). One way to circumvent this limitation is to adopt an iterative procedure for the simulation of the separation distance that may develop between the footing and the supporting soil mound. This can be achieved (for example) by using the elastic half-space foundation model, which is more advanced than Winkler's model for soil-structure interaction problems. However, this model is limited to soil mounds with a constant stiffness profile over depth. But in reality, the soil modulus is greatly affected by both the applied stresses (from the footing) and evolving matric suction [24]. Contact elements is another advanced approach that can be used successfully to simulate complex soil-structure interaction problems. This approach is used in this study to simulate the soil-structure interaction between the soil mound and stiffened slab foundation. The approach allows for the soil-structure separation under tensile stresses and can simulate both the vertical support and lateral friction. Penetration of the footing slab into swelling soil can also be simulated.

According to the Australian Standard AS2870 [13], the maximum design value of the mound stiffness (*Ks*) is 100*q*, where (*q*) is the total building load divided by the area of the slab foundation, with a minimum value is 1000 kPa. For shrinking soils, being dry and hard, the standards proposed a minimum value of 5,000 kPa. In light of this recommendation, the soil mound stiffness (*Ks*) in the current study is reasonably assumed to be 5,000 kPa for the edge drop and 1000 kPa for the edge lift. The footing-soil separation is allowed under tensile stresses and the friction between the soil and footing is simulated using a coefficient of friction of 0.35.

2.3.5 Soil modulus and Poisson's ratio

The stress-strain relationship of an expansive soil is variable and highly dependent on the soil suction [49]. Triaxial compression tests carried out on Black Earth expansive clay from Australia indicated that the soil strength is proportional to the soil suction [49, 50]. The soil elastic modulus (*E*) has a significant impact on the amount of surface heave in numerical modelling; since the suction change is simulated as a change in the mean effective stresses within the soil mass, producing vertical strains as described in Section 2.2. The dependence of (*E*) on the confining pressure is also important to a foundation problem involving soil-structure interaction. However, the effect of (*E*) with respect to the effect of suction is usually marginal, as experimentally confirmed by Hangge et al. [51]. In general, the increase in the (*E*) is more sensitive to the increase in the confining pressure at low suction than at high suction values [52]. The concept of considering the effect of soil suction on (*E*) for reactive soils and neglecting the effect of confining pressure has been previously adopted by many researches [e.g. 17, 19, 24, 53, 54]. However, in this study, the effect of both the soil suction and confining pressure on (*E*) are considered. This is done through a user-defined subroutine, which is developed by the authors and implemented in ABAQUS software used in the current research via which the dependency of the soil modulus-suction and confining pressure is explicitly expressed. In this subroutine, the soil modulus (as a material property) is related to the soil suction (negative pore water pressure) and the confining pressure (as a function of the vertical stresses) based on the study reported by Li [17] and the work carried out by Adem et al. [52]. The negative pore pressure and the confining pressure represent the output of the equilibrium phase of the combined stages of the initial moisture and stress conditions and water precipitation event simulated in the numerical analysis. The user subroutine is generated using Intel Visual Fortran, and a copy is shown in Appendix-A.

By definition, Poisson's ratio (μ) contributes to the volumetric strain in unsaturated soils as shown earlier in Equation 1. The effect of μ on the deflection of footings was reported to be negligible by some researchers [e.g. 55]. However, Li [56] opposed this assumption and proved through FE analyses that the vertical displacement of slab foundations increases with higher values of μ. He attributed this to the fact that, as the value of μ increases, a larger proportion of the lateral swelling strain (which is suppressed by the adjacent soil mass) is transferred into vertical swelling strain and thus increases the slab foundation movement in the vertical direction (i.e. in 1-D manner). It is the view of the authors that, although the value of μ has a direct impact on the absolute deformation of footings, its effect on the differential mound or footing movement is negligible. The value of μ found in the literature for unsaturated clays ranges from 0.2 to 0.4, and μ = 0.3 is reasonably assumed for the swelling soil modelled in this work.

3. Finite element modelling of stiffened slab foundations

It is critically prudent to ensure that the process of finite element (FE) numerical modelling adopted in this work is capable of providing reliable outcomes. To this end, the proposed advanced FE modelling performed in this study is verified against three different stages of case studies. Firstly, the 3D FE modelling is applied to a case study involving field observations of soil mound formation monitoring for a flexible cover membrane. This stage of modelling verification confirms the capability of the adopted hydro-mechanical approach used in the FE modelling in generating realistic soil distorted mound shapes. Secondly, the efficiency of the FE modelling in simulating the water diffusion and suction changes through the soil medium is verified against another case study of corresponding field observations. Thirdly, the FE modelling is applied to hypothetical case study of stiffened slab foundation on reactive soil, and the results are compared with those obtained from Mitchell's method.

All FE models developed in this study are carried out using the commercial software package ABAQUS. This particular software is used due to its ability to conduct a coupled flow-deformation analysis utilising a hydro-mechanical moisture-swell model capable of relating the soil reactivity to degree of saturation and ensuing suction. In this way, the soil distorted mound (a fundamental factor in the design of stiffened slab foundations on reactive soils) is intuitively calculated rather than pre-assumed, a weakness intrinsic to most current available design methods. The calculation of the soil distorted mound in the current FE modelling is based on accurate moisture contours initiated from a transient seepage analysis. The moisture contours generate the corresponding water pore pressure (following the soil-water characteristic curve utilised in the analysis), thereby the volumetric strain simulating the soil heave or shrinkage is readily generated.

3.1 Case study 1: Flexible cover membrane

In this case study, a 3D FE model is developed and checked against field measurements of soil mound formation for a flexible cover membrane resting on an expansive soil in Maryland, Near Newcastle, Australia. This case study involves a field monitoring program carried out by Fityus et al. [57] for the soil movement over a period of 5 years. The configurations of the field test comprise a flexible membrane with dimensions of 10 m × 10 m and the movement monitoring points are located at the middle of the edges and centre of the membrane. Other movement monitoring points are located outside the membrane. Similar to the site set-up, a peripheral beam of 300 mm × 500 mm is generated in the model and a load equivalent to 100 mm of sand is applied on top of the surface of the membrane. The study did not reveal any data for the average seasonal rainfall and evaporation at the site; therefore, these missing data are obtained from the Bureau of Meteorology of Australia (www.bom.gov.au); the data are shown in Fig. 3 (a).

Fig. 3

The soil profile is comprised of 250-350 mm of silty topsoil underlain by high plasticity clay to a depth of approximately 1.0 m, followed by medium plasticity silty clay to a depth of approximately 2.3 m where highly to extremely weathered siltstone is encountered. There is no water table up to 5 m depth. The site is classified as highly expansive (H-class), following the Australian Standard AS 2870 [36], with a characteristic surface heave (y_s) that ranges from 40 mm to 70 mm. In the 3D FE model, the active zone is taken to be 2.5 m, based on the soil stratification. The numerical analysis involves invoking the developed user defined subroutine to achieve the soil modulus and suction dependency.

There is no SWCC available in the geotechnical data but based on the measured suction data and the measured gravitational water content data, some points on the SWCC could be predicted considering a soil specific gravity (G_s) of 2.7, and a soil void ratio (e) of 1.2. The ISWCC proposed in Section 2.3.1 is then found to match fairly well with the measured data, as shown in Fig. 3(b), and is thus used in the FE analysis. The moisture-swell information are also not available in the geotechnical data and the IMSC with a maximum volumetric strain equal to 3%, is thus used, as shown in Fig. 3(c). For better prediction of the surface movement, the IMSC is adjusted to obtain a maximum volumetric strain at saturation values between 40-70 %.

The initial condition of the saturation is set according to the data obtained from the field tests, with a uniform suction over the whole depth of the soil mass equal to 4.7 pF and a degree of saturation of 40 % following the ISWCC. The simulation is carried out in two steps as follows. Firstly, a geostatic analysis is performed in order to set-up the in-situ stresses and nullify the soil deformation caused by the initial suction condition. Secondly, a transient flow-deformation analysis is conducted by applying a time dependent surface load of precipitation and evaporation following the amplitude curve presented in Fig. 3(a), repeated for a period of 5 years. It should be noted that the precipitation value is reduced to 30% owing to the presence of grass and trees in the site, which usually absorb 70% of the rainfall. Similar approach was adopted by Zhang et al. [24] who estimated that the precipitation is usually absorbed by plants. Linear elastic model is used, since there is no need to consider plasticity in such analysis as the focus is on the mound formation. The soil mass is simulated using an 8-node brick, trilinear displacement, trilinear pore pressure element. Fig. 4 shows a snapshot of the FE mesh used in this case study including the soil mass and ground perimeter beam; double symmetry is used in the model.

Fig. 4

In simulating the seepage numerically, the FE size, model boundaries and time increment have to be selected carefully to ensure accuracy of the results. Particularly critical is the choice of the initial time increment in the transient partially saturated flow problem to avoid spurious solution oscillations. The criterion used for a minimum usable time increment in the partial-saturation conditions is expressed as follows:

$$\Delta t > \frac{\gamma n^{o}}{6k_s\, k} \frac{ds}{du} \left(\Delta \ell\right)^2 \tag{11}$$

where;

γ = specific weight of the wetting liquid;

n^o = initial porosity of the material;

k = permeability of the fully saturated material;

k_s = permeability-saturation relationship;

ds/du = rate of change of saturation with respect to pore pressure as defined in the suction profile of the soil material; and

$\Delta\ell$ = typical element dimension.

In general, the size of the model (total soil mass) should be selected so that the boundary conditions have minimum effects on the output results. In this case study, the soil mass plan dimensions is selected with a clear length of 5.0 m away from each edge of the footing. The boundary conditions are set so that the bottom of the soil mass is restrained against the vertical movement, while the sides are restrained horizontally, allowing only for vertical strains. Since swelling can cause significant deformation with respect to the element size, geometric nonlinearity is adopted to account for the effect of large strains on the stiffness matrix formulation; this way the stiffness matrix is adjusted at every time increment when large deformation occurs with respect to the tolerance limits. Interaction properties are defined, between the perimeter ground beams and surrounding soil, allowing for a friction contact with a penalty friction coefficient equal to 0.3.

Fig. 5 shows a comparison between the field observations and FE results, for the movement of two points: one at the centre and another at the edge. It can be seen that the FE results are in good agreement with the field observations. The two selected points show continuous heaving over time, with low tendency to settle even during the dry season, but the points show less tendency to heave towards the end of the observation period. It can also be seen that the point at the centre, being the least affected by the moisture change, suffered the least heave compared to that at the edge, which one would expect. This is attributed to the fact that the water propagates with time towards the centre of the membrane, and the heave at the centre approaches that of the edge at the end of the 5 years. The difference in the heave values between the field observations and FE results may be due to the actual precipitation rates which may differs from the average rate used in the FE analysis.

Fig. 5

Fig. 6(a) shows the progress of the measured mound formation over 5-year observation period, whereas Fig. 6(b) shows the predicted mound formation obtained from the FE analysis. It can be seen from Fig. 6(a) that the ground movement outside the membrane undergoes repeated shrinkage and heave cycles due seasonal variations. On the other hand, the area beneath the cover incurred consistent heave until the initial dry soil becomes wet and approaches its equilibrium water content. Fig. 6(b) shows that the FE results are in general agreement with the field observations; the mound shapes have a prominent dish shape under all climate conditions. In the FE model, the water accumulated beneath the cover membrane caused progressive heave during the course of the 5-year observation period. Numerically, the mound profile shows a drop at the location of the perimeter beams (Fig. 6(b)). According to Fityus et al. [57], the reduction in the swelling at the beam location is due to the reduction of the thickness of the welling soil mass by the depth of the perimeter beams, resulting in a reduction of the final surface heave at these locations.

Fig. 6

The FE model reveals that the differential mound movement between the centre and edges continuously decreases due to the progressive soil wetting beneath the cover. The points located outside the cover membrane are exposed and therefore show cycles of heave and shrinkage; however, their overall dominant movement is heave (Figs. 6(a) and 6(b)). The discrepancies between the FE results and field observations for the points located away from the cover in terms of the higher tendency to shrinkage in the dry season for the field data is most probably due to the presence of trees in the site. This greatly increases the suction and causes much higher shrinkage to the uncovered area than what has been achieved using the evaporation only in the FE analysis. In fact, the large settlements in the open areas cannot be achieved without the transpiration of the tree roots, which is not considered in the FE model.

3.2 Case study 2: Suction simulation

In this course of FE modelling verification, the soil diffusion and suction change with the soil depth in response to the surface suction change is simulated in 3D analysis and verified against field observations for a case study in Amarillo site, Texas. Description of the site conditions is provided by Wray [58]. The soil strata in the site is composed of 3 ft (1.0 m) of low plasticity silty clay, followed by 3 ft (1.0 m) of highly plastic silty clay, and 3 ft (1.0 m) of sandy clay with high plasticity. The third layer is underlain by another very similar light grey clay to at least 27.5 ft (9.1 m), which is slightly sandy and less plastic. The active zone, below which no suction change is observed, is reported to be 13 ft (4.3 m).

The SWCC shown in Fig. 7(a) is used in the FE modelling for this site. In this case, the SWCC is developed based on best fit to measured data. Since there is no measured moisture swell curve, the IMSC curve is used with a maximum volumetric strain of 1.5%, as shown in Fig. 7(b). The site has a covered area of 11.0 m × 15.8 m, and the model dimensions are extended to a distance of 5.0 m outside the cover membrane. The suction change over the time period of 5 years using Equation 4 is applied all around the covered area, with an initial uniform suction of 4.5 pF. The double symmetry is again used in the FE model. Fig. 8 shows the 3D FE model highlighting the area of the surface suction change.

Fig. 7

Fig.8

Fig. 9 illustrates the predicted and measured suction variation with time for points located at 0.9 m outside the covered area at depths 0.9 m [Fig. 9(a)] and 2.1 m [Fig. 9(b)]; and at 3.0 m inside the covered area at depths of 0.9 m [Fig. 9(c)] and 2.1 m [Fig. 9(d)], along the long dimension of the cover membrane. In general, the predicted values of the suction change with time agree reasonably well with the measured values (the suction change diminish with time and depth), despite the fact that the measured values are a bit higher presumably due to the presence of grass and cracks in the site. Grass evaporation increases the suction while cracks provide easy access for the surface water into the soils, hence, affecting the amount of diffusion.

Fig. 9

Fig. 10 illustrates a comparison between the measured and FE predicted soil movement with time for points located at the surface, 1.8 m outside the covered area along the short direction and a point located at 0.6 m from the centre of the covered area along the long axis. It can be seen that the predicted movements with time for both the point located outside the cover area [Fig. 10(a)] and the point located inside the cover area [Fig. 10(b)] agree fairly well with the measured data and the variation trends are well captured by the FE model, indicating a good modelling prediction capability.

Fig. 10

3.3 Case study 3: Hypothetical Stiffened Slab Foundation

In this section, the efficacy of the FE coupled flow-deformation analysis in simulating the behaviour of stiffened slab foundations for light-weight structures on expansive soils is investigated. To this end, the results of the FE modelling are compared with Mitchell's method, which is one of the most commonly used design methods currently adopted by the Australian Standard AS2870 [13]. Since Mitchell's method adopts 2D analysis, a 2D FE model is firstly generated for verification with Mitchell's method, then a more realistic 3D FE model is developed for the purpose of comparison with the 2D analysis.

A stiffened slab foundation usually comprises a concrete raft (mat), typically 100 mm thick, stiffened with ground beams casted monolithically with the slab, with a spacing less than 4.0 m apart. Both the dimensions of the ground beams and amount of reinforcement depend on the estimated level of soil movement. In this case study, a hypothetical slab stiffened foundation of dimensions (16 m × 8 m) is assumed to be supporting an articulated masonry veneer of a single storey building. The footing slab is 100 mm thick and stiffened with ground beams spaced at 4 m apart in each direction (i.e. total of 5 beams having 8 m span and 3 beams having 16 m span). Each beam has a width of 300 mm; the requirement is to determine the depth that can sustain the internal forces induced by the volumetric change resulting from the moisture variation. The footing slab is resting on 4.0 m highly reactive soil class H-D, following the classification of the Australian Standard AS 2870 (2011), with an expected surface characteristic heave (y_s) of 70 mm. The footing slab is subjected to a uniform load comprising the finishing and long term live loads of 1.5 kPa. An edge load of 6.0 kN/m′ is applied on the perimeter, simulating the loads from the edge walls and roof. For the articulated masonry veneer, the Australian Standard AS 2870 [13] allows for a maximum footing differential movement equal to $L/400 \leq 30$ mm (where; L is the footing dimension in the direction under consideration). The differential mound movement (y_m) is considered in accordance with the Australian Standard AS2870 [13] to be 70% of the characteristic surface heave (i.e. y_m = 0.7 y_s = 49 mm). Normal contact penalty stiffness of 1,000 kPa and 5,000 kPa simulating the soil mound stiffness under the edge lift and edge drop, respectively, are assumed following the recommendation of the Australian Standard AS2870 [13].

The footing stiffness (EI) required to limit the differential movement to the standard requirement is first calculated using Mitchell's method. By considering a concrete elastic modulus = 15,000 MPa, the required beam depth of the stiffened footing is calculated. In the design of the stiffening beam for the case of edge heave (i.e. slab in compression), a T-section is considered with an equivalent flange width = 0.1 L, whereas for the case of edge settlement (i.e. slab in tension) a rectangular section for the stiffened beam is considered. The calculation is carried out for the edge lift and edge drop for the footing two spans (i.e. 16.0 m and 8.0 m) separately. Table 1 summarises the required equivalent footing slab thickness (having same inertia as the stiffened slab) calculated from Mitchell's method.

Table 1

The same footing slab stiffness obtained from Mitchell's method are then used in the 2D FE model. In real design, the maximum inertia would be used; however, in this study the same slab inertia calculated by Mitchell's method for each heaving scenario is utilised for the purpose of comparison with the FE modelling. A linear elastic material is used for both the footing slab and the swelling clay layer, since the focus is on the volumetric response due to swelling (refer to Table 2). This assumption is reasonable, because light-weight structures are expected to produce stresses that are relatively low anyway. The permeability of the clay layer and rate of precipitation are assumed to be 1.0 × 10^{-9} m/s and 3.8 × 10^{-8} m/s (about 100 mm/month), respectively.

Table 2

The initial void ratio of the swelling clay is taken as 1.2. The idealised moisture-swell curve (IMSC) shown earlier in Fig. 2 is used in the FE modelling. The flow period for the edge lift and the evaporation period for the edge drop are imposed to achieve the target differential mound movement (i.e. y_m = 49 mm), based on the pre-calculated slab thickness using Mitchell's method. The boundary conditions of the FE model are set to restrict the vertical displacement at the bottom of the model, while no lateral movement is allowed at the vertical sides. The initial saturation and suction conditions are set following the idealised soil-water characteristic curve (ISWCC) shown earlier in Fig. 1, so that the initial conditions of the edge lift are set to be dry (i.e. saturation = 40 % and uniform suction = 4.69 pF) over the depth of the soil mass, whereas these conditions for the edge drop are set to be wet (i.e. saturation = 95% and uniform suction = 3.0 pF).

The time increment is chosen to allow for monitoring the mound formation and pointing the time required to achieve the target differential mound movement (i.e. y_m = 49 mm). The geometric nonlinearity is considered as explained in the previous sections. The modelling is performed in 3 steps. In the first step, a geostatic analysis is carried out as in the previous validation examples (Case Study 2) to eliminate the deformation of the initial suction and allow for the set-up of the in-situ stresses. In the second step, the loading of the slab foundation is applied, including all uniform loads, edge line loads and self-weight. In the third step, the flow or evaporation inducing the edge lift or edge drop is activated. It should be noted that the self-weight of the slab foundation, which is simulated as a plate of uniform thickness, is adjusted to consider the actual self-weight of an equivalent stiffened slab having the same inertia. Figs. 11

and 12 show the deformed shape of the 2D FE model in the long and short footing slab dimensions, under the edge lift and edge drop scenarios, respectively.

Fig. 11

Fig. 12

In reality, the mound shape forms a complicated three-dimensional surface [59, 60]. This particular feature highlights the power of the FE modelling in reproducing and carrying out a more realistic coupled 3D flow-deformation and stress analysis. This feature can overcome the 2D major assumption adopted by most existing methods, eliminating the need to undertake the analysis of the footing slab in each direction separately, which invariably violates the deformation compatibility of the soil and footing. For instance, if a rectangular slab is analysed using the 2D analysis, the analysis would consider different values for the maximum differential mound movement (y_m) in each direction, being the difference between the soil beneath the centre of the footing and the soil beneath the edge of the footing. However, under the more realistic 3D analysis, the footing would be analysed as a plate resting on a 3D mound having a maximum differential mound movement (y_m) as being the difference between the soil beneath the centre of the footing and the soil beneath the corner of the footing. Consequently, for the deformation compatibility, the maximum differential mound movement between the centre and edges (either in the long or short span) would be much less than the target (y_m) used in the 2D analysis and accordingly the required inertia that limits the deformation would thus be reduced.

In the 3D FE analysis, the same case study used in the 2D FE analysis, with the same maximum differential mound movement, is considered. However, the maximum differential mound movement is defined to be the difference in movement between the soil beneath the centre of the footing and the soil beneath the corner of the footing, as mentioned above. Fig. 13 shows a snapshot of the 3D FE model.

Fig. 13

Under both the edge lift and edge drop scenarios, the maximum allowable footing movement (i.e. $L/400 \leq 30$ mm) is achieved by using a slab foundation of uniform thickness = 200 mm. Compared with the maximum thickness obtained from the 2D FE analysis (i.e. 350 mm), the 200 mm slab thickness obtained from the 3D analysis is found to achieve a considerable reduction in the slab foundation thickness for the loading conditions used. Fig. 14 demonstrates the deformed shapes of the soil and footing in the 3D FE analysis.

Fig. 14

Figs. 15-18 present comparisons between the output obtained from Mitchell's method and the 2D and 3D FE analyses for a 1.0 m strip parallel to the flow direction, in both the edge lift and edge drop scenarios. It can be seen from all figures that the overall results of the 2D FE analysis and Mitchell's method agree fairly well. Under the edge lift scenario, in the long footing span, the soil mound is flatter in the 2D FE analysis than Mitchell's method, while in the short footing span both methods produced similar soil movements. The footing slab thicknesses calculated by Mitchell's method showed similar footing deformation to that of the 2D FE analysis. The bending moment obtained from Mitchell's method in the long direction slightly exceeds that obtained from the 2D FE due to the difference in the soil mound, which provided less support to the footing in Mitchell's method. Similar to the bending moment, the shear force values of the 2D FE analysis are very close to those obtained from Mitchell's method, for both the edge lift and edge drop scenarios.

The soil mound differential movements obtained from the 3D FE analysis are significantly less than those obtained from both the 2D FE analysis and Mitchell's method. This is attributed to the way the 3D FE analysis handles the differential movement between the centre and edges in each case, as mentioned above. In other words, the reason is due to the lack of compatibility in Mitchell's method and 2D FE analysis, compared with the 3D FE analysis. The compatibility effect is expressed in the slab spatial bending that distributes the acting loads rather than in one direction as in the 2D FE analysis and Mitchell's method. The end result is less internal forces for the 3D analysis under the edge lift and edge drop scenarios, as shown in the bending moment and shear force diagrams.

Figs. 15 to 18

4. Conclusions

The behaviour of stiffened slab foundations on expansive soils (including formation of the distorted soil surface beneath the footing) due to moisture precipitation or evaporation depends on many parameters such as the soil-water suction characteristics (called here the SWCC), moisture-swell characteristics, soil permeability/duration of flow, initial saturation/suction conditions, soil modulus and footing loads. In this paper, an advanced FE modelling using a hydro-mechanical approach and coupled flow-deformation analysis was performed involving the abovementioned parameters, which are the thrust of the current work. The proposed FE modelling was verified through three cases studies. The first case study involved field observations of soil mound formation of a flexible cover membrane resting on a highly expansive soil over a period of 5 years in Newcastle, Australia. The mound formation over the course of observations was found to be similar to the FE analysis. This stage of modelling confirmed the reliability of the adopted FE modelling in generating realistic soil distorted mound shapes. The second case study presented field observations of the suction change and soil movement for a site in Amarillo, Texas. The results of the FE modelling agreed fairly well with the field observations, which verified the efficiency of the FE modelling in simulating the water diffusion and suction change through the soil medium. The third case study involved a hypothetical stiffened slab foundation on reactive soil, which was solved using 2D/3D FE modelling and compared with Mitchell's method. The 2D FE analysis showed good agreement with Mitchell's method. However, the 3D FE analysis developed more realistic mound shapes and achieved deformation compatibility; a matter that is usually disregarded in the 2D analysis adopted by most existing design methods.

The results presented in this paper provided insights into the capability of the proposed 3D coupled flow-deformation and stress analysis in realistically simulating the behaviour of stiffened slab foundations on expansive soils, overcoming some major limitations inherent in most existing methods. These include: (i) realistic formation of 3D soil mounds, based on coupled seepage and deformation analyses, rather than the pre-defined 2D soil mounds adopted in the exiting previous methods; and (ii) simultaneous stress analysis and transient seepage, by involving the effect of suction change on the soil stiffness and implementing representative contact elements for the soil-footing interaction. In future subsequent phase of this work, a comprehensive parametric study involving different slab foundation dimensions (using the same 3D FE set-up developed in this paper) will be carried out with the intention to develop design charts and procedures that can be readily used for design purposes by engineers and practitioners.

Acknowledgment

The authors would like to acknowledge the contribution of the Australian Government Research Training Program Scholarship in supporting this research.

Appendix A

A1: User Defined Subroutine "USDFLD"

```
      SUBROUTINE USDFLD(FIELD,STATEV,PNEWDT,DIRECT,T,CELENT,
     1 TIME,DTIME,CMNAME,ORNAME,NFIELD,NSTATV,NOEL,NPT,LAYER,
     2 KSPT,KSTEP,KINC,NDI,NSHR,COORD,JMAC,JMATYP,MATLAYO,
     3 LACCFLA)
C
      INCLUDE 'ABA_PARAM.INC'
C
      CHARACTER*80 CMNAME,ORNAME
      CHARACTER*3  FLGRAY(15)
      DIMENSION FIELD(NFIELD),STATEV(NSTATV),DIRECT(3,3),
     1 T(3,3),TIME(2)
      DIMENSION ARRAY(15),JARRAY(15),JMAC(*),JMATYP(*),
     1 COORD(*)
C
      CALL GETVRM('Por',ARRAY,JARRAY,FLGRAY,JRCD,JMAC,JMATYP,
     1 MATLAYO,LACCFLA)
      Por = ARRAY(1)
C   Use the pore pressure as a field variable
       FIELD(1) = ARRAY(1)
C    Store the Pore Pressure as a solution dependent state
C    variable
        STATEV(1) = FIELD(1)
```

```
      RETURN
      END
```

A2: Keyword File for Soil Modulus Dependency

```
** MATERIALS
*Material, name=Swelling-soil
*Elastic, dependencies=2
 5.0e7, 0.3, 50,-3.9e6
5.5e7, 0.3, 100,-3.9e6
6.0e7, 0.3, 150,-3.9e6
4.0e7, 0.3, 50,-1.6e6
4.6e7, 0.3, 100,-1.6e6
5.3e7, 0.3, 150,-1.6e6
3.0e7, 0.3, 50,-650000
3.8e7, 0.3, 100,-650000
4.6e7, 0.3, 150,-650000
2.0e7, 0.3, 50,-250000
3.0e7, 0.3, 100,-250000
4.0e7, 0.3, 150,-250000
1.1e07, 0.3, 50,-250000
2.2e07, 0.3, 100,-250000
3.4e07, 0.3, 150,-250000
*USER DEFINED FIELD
*DEPVAR
2
```

References

[1] Krohn JP, Slosson JE. Assessment of expansive soils in the United States. Proceedings of the 4^{th} International Conference on Expansive Soils. Denver, Colorado, USA. 1980:596-608.

[2] Nuhfer EB. What’s a geologic hazard? Geotimes. 1994; 39 (7):4.

[3] Wray WK. So your home is built on expansive soils: a discussion of how expansive soils affect buildings. Virginia, USA: American Society of Civil Engineers, 1995.

[4] Robert L, Andrew B, Mary LC. Soils shrink, trees drink, and houses crack. ECOS Magazine: The Science Communication Unit of CSIRO's Bureau of Scientific Services, 1984. p. 13-5.

[5] Building Research Advisory Board. Criteria for selection and design of residential slabs on ground. 1968; Report No. 33.

[6] Lytton RL. Analysis for design of foundations on expansive clay. Proceedings of the Symposium of Soils & Earth Structures in Arid Climates. Adelaide, Australia. 1970:29-37.

[7] Walsh PF. The design of residential slab on ground. 1974; Technical Report No. 5.

[8] Mitchell PW. The structural analysis of footings on expansive soil. Proceedings of the 4^{th} International Conference on Expansive Soils. Denver, Colorado, USA. 1980;1:438-47.

[9] Holland JE, Cimino DJ, Lawrance CE, Pitt WG. The behaviour and design of housing slabs on expansive clays. Proceedings of the 4^{th} International Conference on Expansive Soils. Denver, Colorado, USA 1980;1:448-68.

[10] Post Tensioning Institute. Design and construction of post-tensioned slabs-on-ground. 2^{nd} Edition. 1996.

[11] Wire Reinforcement Institute. Design of slab-on-ground foundations. 1981.

[12] Wire Reinforcement Institute. Design of slab-on-ground foundations. 1996.

[13] Australian Standard AS2870. Residential slabs and footings. Sydney NSW: Standard House, 2011.

[14] Fraser RA, Wardle LJ. The analysis of stiffened raft foundations on expansive soil. Symposium on Recent Developments in the Analysis of Soil Behaviour and their Application to Geotechnical Structures. University of New South Wales, Australia. 1975:89-98.

[15] Poulos HG. Analysis of strip footings on expansive soils. 1983; Report No. R459.

[16] Sinha J, Poulos HG. Behaviour of stiffened raft foundations. 7th Australia New Zealand Conference on Geomechanics: Geomechanics in a Changing World. Barton, ACT. 1996:704-9.

[17] Li J. Analysis and modelling of performance of footings on expansive soils [PhD Thesis]. Australia: University of South Australia, 1996.

[18] El-Garhy BM, Wray WK. Method for calculating the edge moisture variation distance. Journal of Geotechnical and Geoenvironmental Engineering. 2004; 130 (9):945-55.

[19] Wray WK, El-Garhy BM, Youssef AA. Three-dimensional model for moisture and volume changes prediction in expansive soils. Journal of Geotechnical and Geoenvironmental Engineering. 2005; 131 (3):311-24.

[20] Fredlund MD, Stianson JR, Fredlund DG, Vu H, Thode RC. Numerical modeling of slab-on-grade foundations. Proceedings of the 4th International Conference on Unsaturated Soils. Arizona, USA. 2006;2:2121-32.

[21] Abdelmalak RI. Soil structure interaction for shrink-swell soils. new design procedure for foundation slabs on shrink-swell soils [PhD Thesis]. Texas, USA: Texas A&M University, 2007.

[22] Magbo C. Design method for stiffened slab on grade placed on shrink-swell soils and subjected to uniform pressure and line loads [Master's Thesis]. Texas, USA: A&M University, 2014.

[23] Dafalla MA, Al-Shamrani MA, Puppala AJ, Ali HE. Design guide for rigid foundation systems on expansive soils. International Journal of Geomechanics. 2011; 12 (5):528-36.

[24] Zhang X, Briaud JL. Three dimensional numerical simulation of residential building on shrink–swell soils in response to climatic conditions. International Journal for Numerical and Analytical Methods in Geomechanics,. 2015; 39 (13):1369-409.

[25] Adem HH, Vanapalli SK. Review of methods for predicting in situ volume change movement of expansive soil over time. Journal of Rock Mechanics and Geotechnical Engineering. 2015; 7 (1):73-86.

[26] Fredlund DG, Morgenstern NR. Constitutive relations for volume change in unsaturated soils. Canadian Geotechnical Journal. 1976; 13 (3):261-76.

[27] Gay DA. Development of a predictive model for pavement roughness on shrink-swell clay [PhD Thesis]. Texas, USA: A&M University, 1993.

[28] Wray WK. Development of a design procedure for residential and light commercial slabs-on-ground constructed over expansive soils [PhD Thesis]. Texas, USA: Texas A&M University, 1978.

[29] Briaud JL, Abdelmalak R, Zhang X. Design of stiffened slabs-on-grade on shrink-swell soils. Proceedings of the 5th International Conference on Unsaturated Soil. Barcelona, Spain. 2010.

[30] Puppala AJ, Manosuthikij T, Chittoori BC. Swell and shrinkage characterizations of unsaturated expansive clays from Texas. Engineering Geology. 2013; 164:187-94.

[31] Pulat HF, Yukselen-Aksoy Y, Egeli I. The effect of soil mineralogy and pore fluid chemistry on the suction and swelling behavior of soils. Bulletin of Engineering Geology and the Environment. 2014; 73 (1):37-42.

[32] Williams PJ. The surface of the Earth: An introduction to geotechnical science. New-York: Longman Inc., 1982.

[33] Fredlund DG, Xing A. Equations for the soil-water characteristic curve. Canadian Geotechnical Journal. 1994; 31 (4):521-32.

[34] Vanapafli SK, Fredlund DG, Pufahl DE. The influence of soil structure and stress history on the soil-water characteristics of a compacted till. Geotechnique. 1999; 49 (2):143-59.

[35] Mitchell PW. The design of shallow footings on expansive soil. [PhD Thesis]. Australia: University of Adelaide, 1984.

[36] Australian Standard AS2870. Residential slabs and footings. Sydney NSW: Standard House, 1996.

[37] Mitchell PW. Footing design for residential type strctures in arid climates. Australian Geomechanics. 2008; 43 (4):51-68.

[38] ABAQUS User's Manual. Version 6.14: Moisture Swelling. 1080 Main Street, Pawtucket, RI02860-4847, U.S.A: Hibbit, Karlsson and Sorenson Inc., 2014.

[39] Tripathy S, Rao KS, Fredlund DG. Water content-void ratio swell-shrink paths of compacted expansive soils. Canadian Geotechnical Journal. 2002; 39 (4):938-59.

[40] Kodikara JK, Choi X. A simplified analytical model for desiccation cracking of clay layers in laboratory tests. Proceedings of the 4th International Conference on Unsaturated Soils. Carefree, Arizona. 2006:2558-69.

[41] Al-Shamrani MA, Dhowian AW. Experimental study of lateral restraint effects on the potential heave of expansive soils. Engineering Geology. 2002; 69 (1):63-81.

[42] Chen FH. Foundations on expansive soils. New York: Elseiver Science Publishing Company INC, 1988.

[43] Thakur VK, Singh DN. Rapid determination of swelling pressure of clay minerals. Journal of Testing and Evaluation. 2005; 33 (4):239-45.

[44] Fredlund DG, Rahardjo H. Soil mechanics for unsaturated soils. New York, USA: John Wiley & Sons, 1993.

[45] Richards BG. Moisture flow and equilibria in unsaturated soils for shallow foundations-Special technical publication no. 417. Symposium on Permeability and Capillarity of Soils. Philadelphia, USA. 1967:4-34.

[46] Fredlund DG, Rahardjo H. An overview of unsaturated soil behaviour. Proceedings of the American Society of Civil Engineers , Geotechnical Special Publication on Unsaturated Soil Properties. Dallas, Texas, USA. 1993:1-31.

[47] Forchheimer P. Wasserbewegung durch boden (water movement through soil). Germany: Z. Ver. Deutsch. Ing. 45, 1901.

[48] Mitchell JK, Hooper DR, Campanella RG. Permeability of compacted clay. Journal of Soil Mechanics & Foundations Division. 1965; SM4 (91):41-65.

[49] Richards BG, Gordon R. Prediction and observation of the performance of a flexible pavement on expansive clay subgrade. 3rd International Conference on the Structural Design of Asphalt Pavements. London, England. 1972;1:11-5.

[50] Li J, Cameron DA, Symons MG. Three-dimensional analysis of stiffened slabs on expansive soils Proceeding of International Conference on Computational Methods in Engineering. Singapore. 1992:119-204.

[51] Hangge EE, Hardiyatmo HC, Adi AD, Rifa'i A. Influence of swell on stress-strain behaviour of expansive soils under confining pressure. International Organization of Scientific research, Journal of Engineering. 2015; 05 (06):48-54.

[52] Adem HH, Vanapalli SK. Prediction of the modulus of elasticity of compacted unsaturated expansive soils. International Journal of Geotechnical Engineering. 2015; 9 (2):163-75.

[53] Briaud JL, Abdelmalak R, Xiong Z, Magbo C. Stiffened slab-on-grade on shrink-swell soil: New design method. Journal of Geotechnical and Geoenvironmental Engineering. 2016; 142 (7):04016017.

[54] Li J, Cameron DA, Ren G. Case study and back analysis of a residential building damaged by expansive soils. Computers and Geotechnics. 2014; 56: 89-99.

[55] Pidgeon JT. The interaction of expansive soil and a stiffened raft foundation. Proceedings of the 7th Regional Conference for Africa on Soil Mechanics and Foundation Engineering. Ghana. 1980:811-22.

[56] Li J. Finite element analysis of deep beams in expansive clays. 1st International Conference on Unsaturated Soils. Paris, France 1995:1109-15.

[57] Fityus SG, Allman MA, Smith DW. Mound shapes beneath covered areas. Proceedings of the 8th Australia New Zealand Conference on Geomechanics: Consolidating Knowledge. Barton, ACT. 1999:163-70.

[58] Wray WK. Mitigation of damage to structures supported on expansive soils. 1990;1; Report No. Eke-8320493.

[59] Walsh PF, Walsh SF. Structure/reactive clay model for a microcomputer. 1986; Report No. 86/9.

[60] Pile KC. The deformation of structures on reactive clay soils. 5th International Conference on Expansive Soils. Barton, ACT. 1984:292-9.

Figure captions:

Fig. 1. Idealised soil-water characteristic curve (ISWCC) for empirical parameters: a = 1000, m = 1.25 and n = 1 (Site 1: Paris Soil Data[30]; Site 2: Houston Soil Data [30]; Site 3: Regina Clay [33]; Site 4: Fort Worth Soil [30]; Site 5: Kidd Greek Tailings [33]).

Fig. 2. Idealised moisture-swell curve used in the current study.

Fig. 3. Data used for modelling Newcastle site of Case Study (1)**:** (a) Rainfall and evaporation rates in Newcastle, Australia (www.bom.gov.au); (b) Measured and proposed ISWCC; and (c) Idealised moisture-swell curve

Fig. 4. Finite element mesh and area of moisture change around the flexible cover membrane of Case Study (1).

Fig. 5. FE results and observed data for movement with time for some selected points on the flexible cover membrane of Case Study (1).

Fig. 6. Mound formation with time for Case Study (1): (a) Observed mound (redrawn from Fityus et al. [57]); and (b) FE predicted mound**.**

Fig. 7. Data used for modelling Amarillo site of Case Study (2): (a) SWCC; and (b) IMSC.

Fig. 8. FE mesh and boundary of surface suction change used for modelling Amarillo site of Case Study (2).

Fig. 9. Measured versus FE predicted suction changes at Amarillo site of Case Study (2), for points located at 0.9 m outside the covered area at depths: (a) 0.9 m; and (b) 2.10 m. And for points located at 3.0 m inside the covered area at depths: (c) 0.9 m; and (d) 2.10 m.

Fig. 10. Measured versus FE predicted surface movements at Amarillo site of Case Study (2), for points located at: (a) 1.8 m outside the covered area along the short axis; and (b) 0.6 m from the cover centre along the longitudinal axis.

Fig. 11. 2D FE results of Case Study (3) showing the soil and footing movements in the long span: (a) edge lift scenario; and (b) edge drop scenario (*legend values in metres*).

Fig. 12. 2D FE results of Case Study (3) showing the soil and footing movements in the short span: (a) edge lift scenario; and (b) edge drop scenario (*legend values in metres*).

Fig. 13. 3D FE model of Case Study (3).

Fig. 14. Deformed shapes of 3D FE model for Case Study (3): (a) edge drop scenario; and (b) edge lift scenario (*legend values in metres*).

Fig. 15. Comparison between Mitchell's method and 2D/3D FE soil movement results of Case Study (3): (a) long footing span (edge lift scenario); (b) long footing span (edge drop scenario); (c) short footing span (edge lift scenario); and (d) short footing span (edge drop scenario).

Fig. 16. Comparison between Mitchell's method and 2D/3D FE footing movement results of Case Study (3): (a) long footing span (edge lift scenario); (b) long footing span (edge drop scenario); (c) short footing span (edge lift scenario); and (d) short footing span (edge drop scenario).

Fig. 17. Comparison between Mitchell's method and 2D/3D FE bending moment results of Case Study (3): (a) long footing span (edge lift scenario); (b) long footing span (edge drop scenario); (c) short footing span (edge lift scenario); and (d) short footing span (edge drop scenario).

Fig. 18. Comparison between Mitchell's method and 2D/3D FE shear force results of Case Study (3): (a) long footing span (edge lift scenario); (b) long footing span (edge drop scenario); (c) short footing span (edge lift scenario); and (d) short footing span (edge drop scenario).

<u>Table captions:</u>

Table 1. Summary results obtained from Mitchell's method.

Table 2. Parameters of finite element modelling used for Case Study (3).

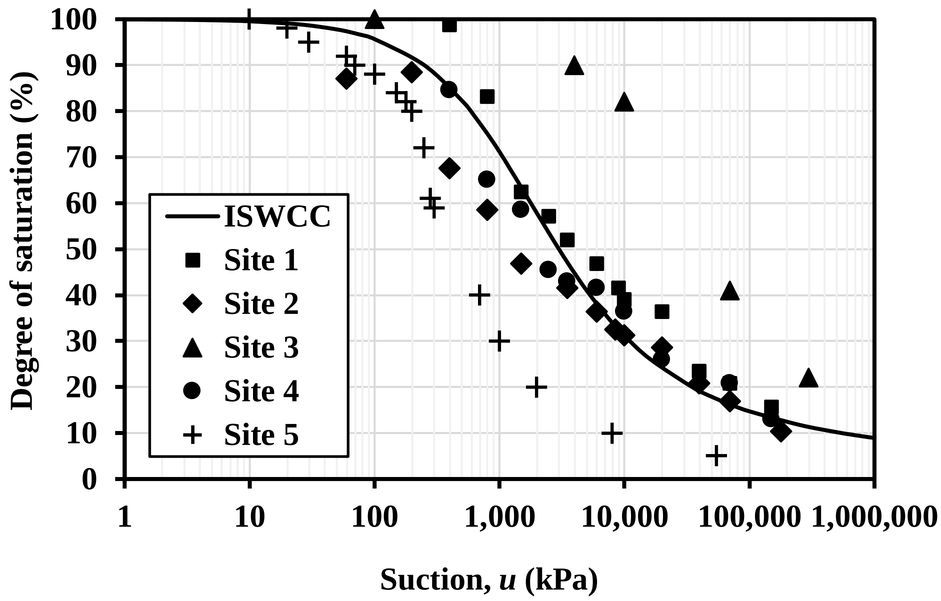

Degree of saturation (%)
100
90
80
70
60
50
40
30
20
10
0
1
10
100
1,000
10,000
100,000
1,000,000
Suction, u (kPa)
ISWCC
Site 1
Site 2
Site 3
Site 4
Site 5

Fig. 1

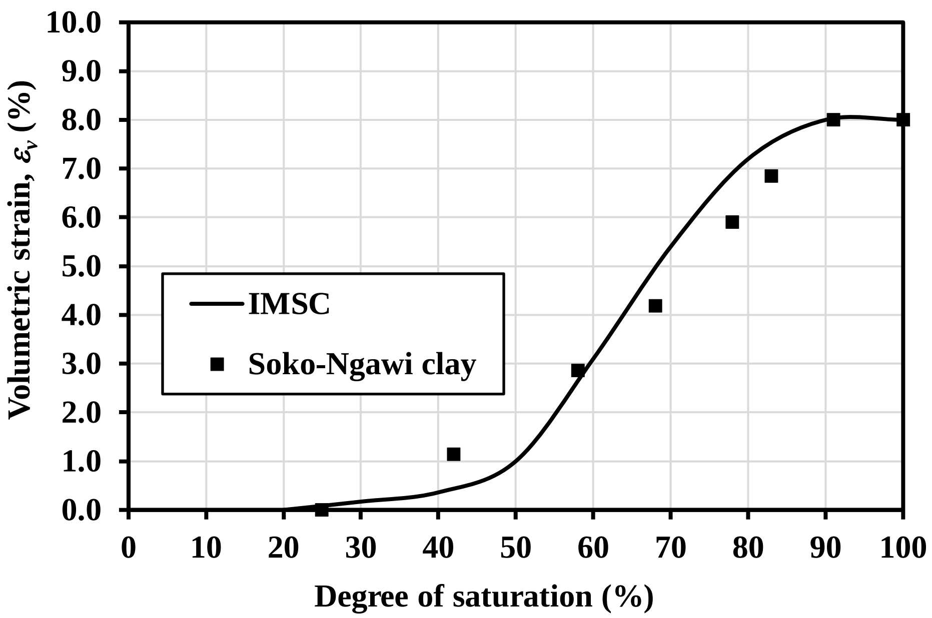

Volumetric strain, εv (%)
10.0
9.0
8.0
7.0
6.0
5.0
4.0
3.0
2.0
1.0
0.0
0
10
20
30
40
50
60
70
80
90
100
Degree of saturation (%)
IMSC
Soko-Ngawi clay

Fig. 2

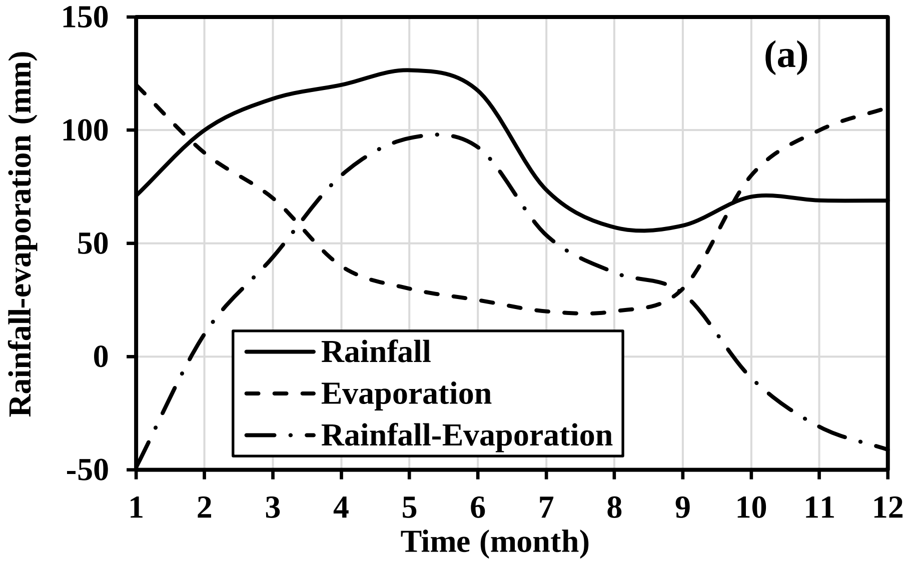
150
100
50
0
-50
(a)
Rainfall
Evaporation
Rainfall-Evaporation
Rainfall-evaporation (mm)
1 2 3 4 5 6 7 8 9 10 11 12
Time (month)

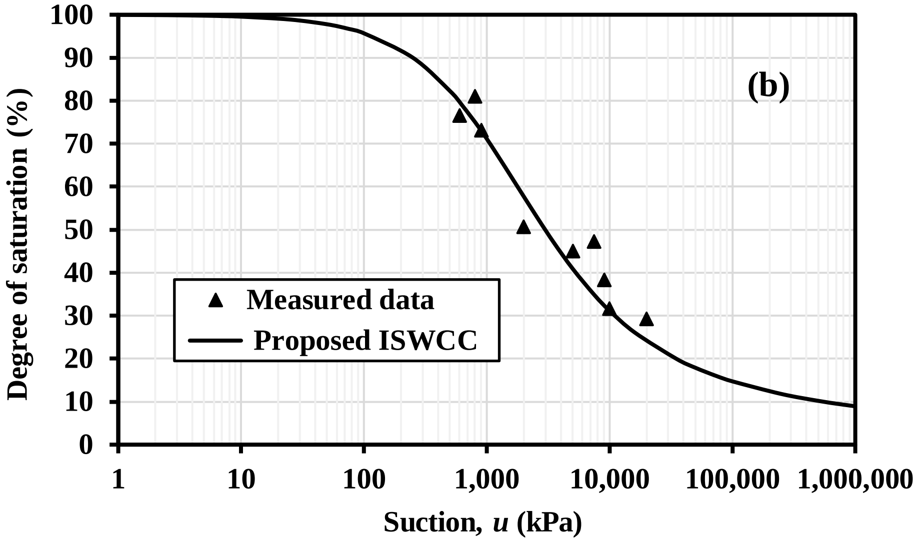
100
90
80
70
60
50
40
30
20
10
0
(b)
Measured data
Proposed ISWCC
Degree of saturation (%)
1 10 100 1,000 10,000 100,000 1,000,000
Suction, u (kPa)

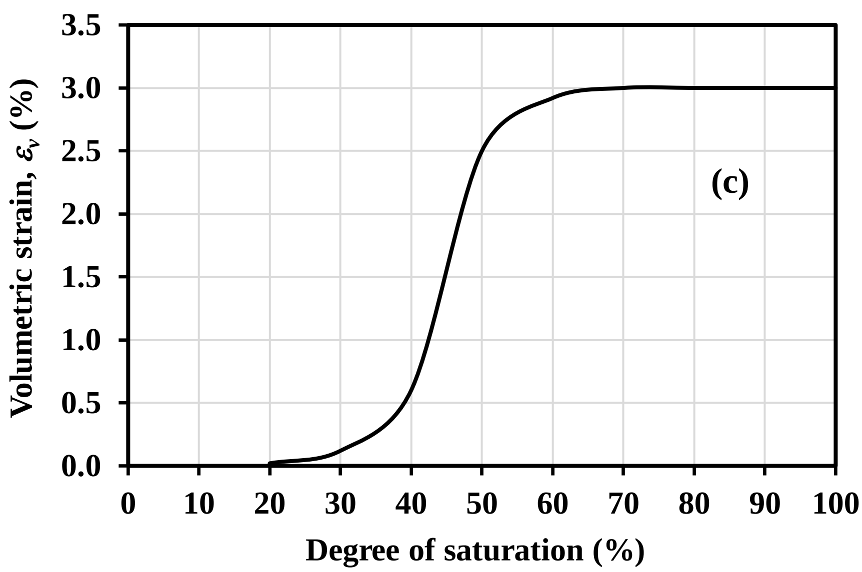
3.5
3.0
2.5
2.0
1.5
1.0
0.5
0.0
(c)
Volumetric strain, ε_v (%)
0 10 20 30 40 50 60 70 80 90 100
Degree of saturation (%)

Fig. 3

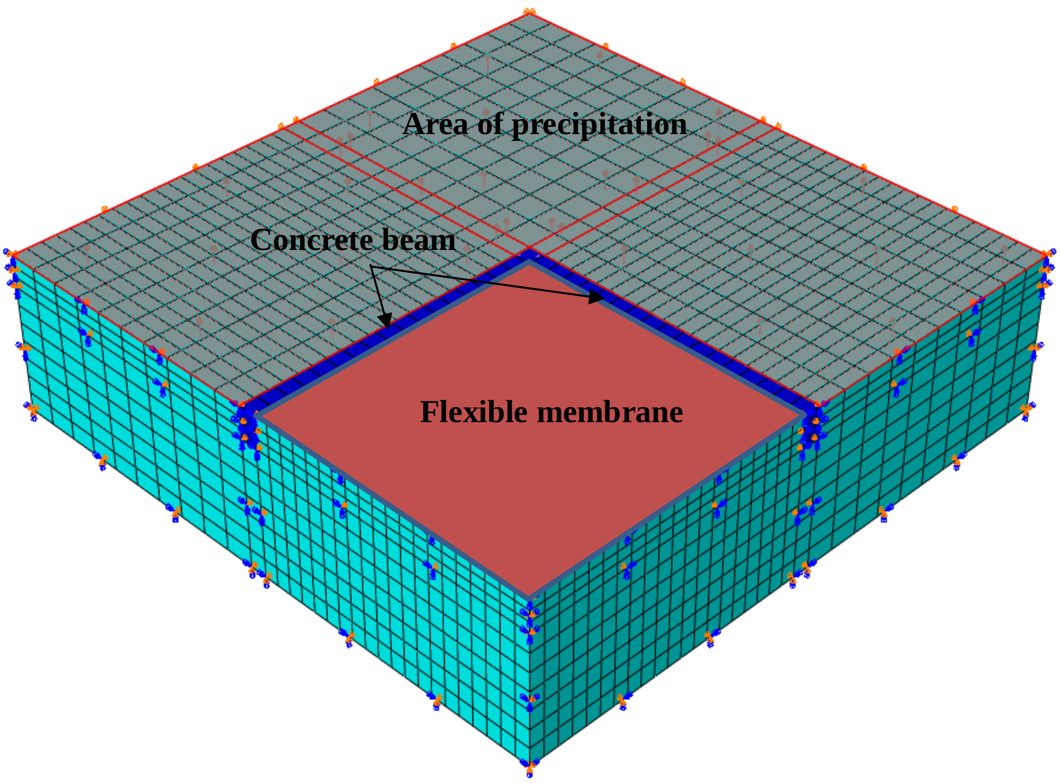

Area of precipitation
Concrete beam
Flexible membrane

Fig. 4

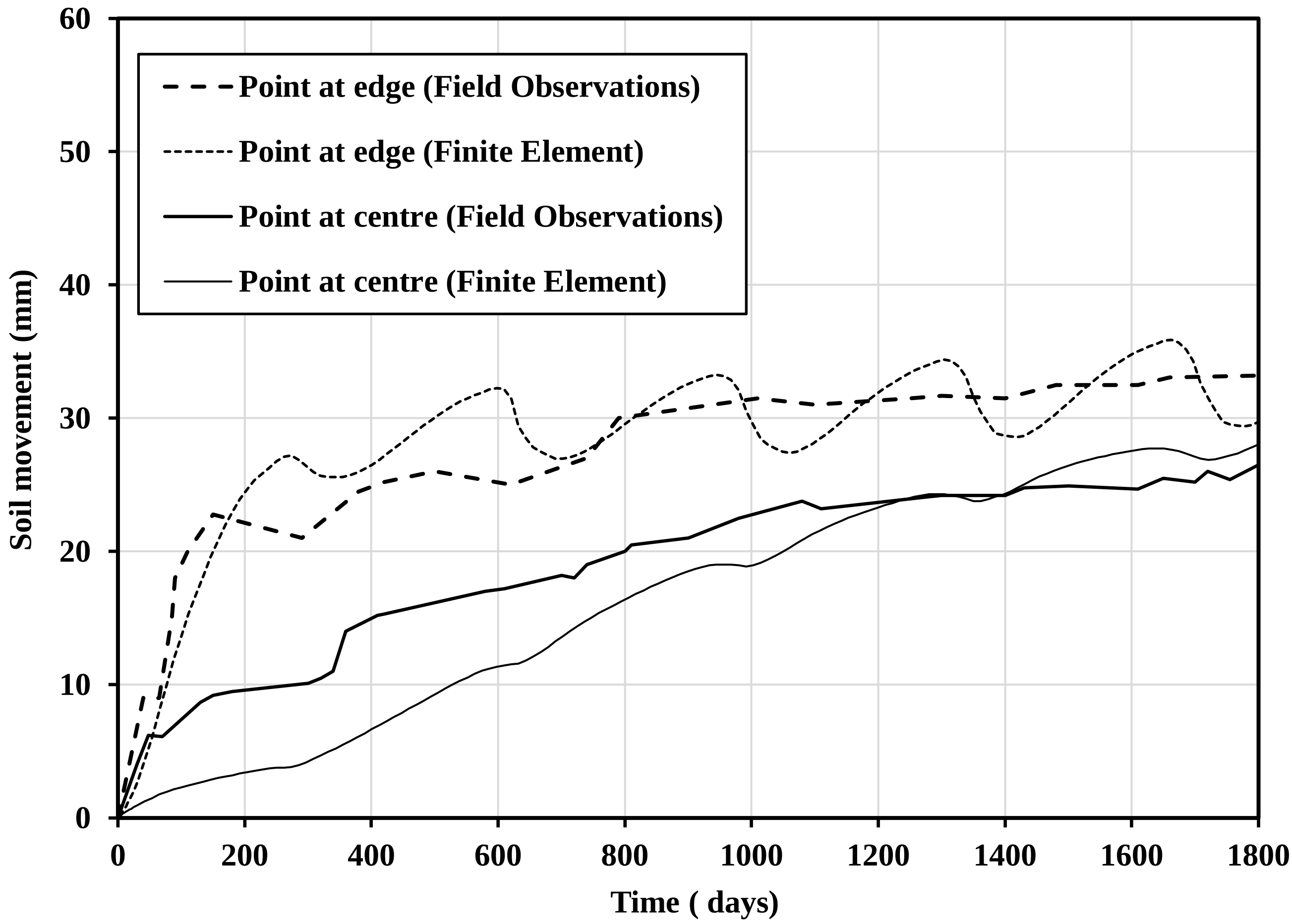

Point at edge (Field Observations)
Point at edge (Finite Element)
Point at centre (Field Observations)
Point at centre (Finite Element)
Soil movement (mm)
Time (days)
0
10
20
30
40
50
60
200
400
600
800
1000
1200
1400
1600
1800

Fig. 5

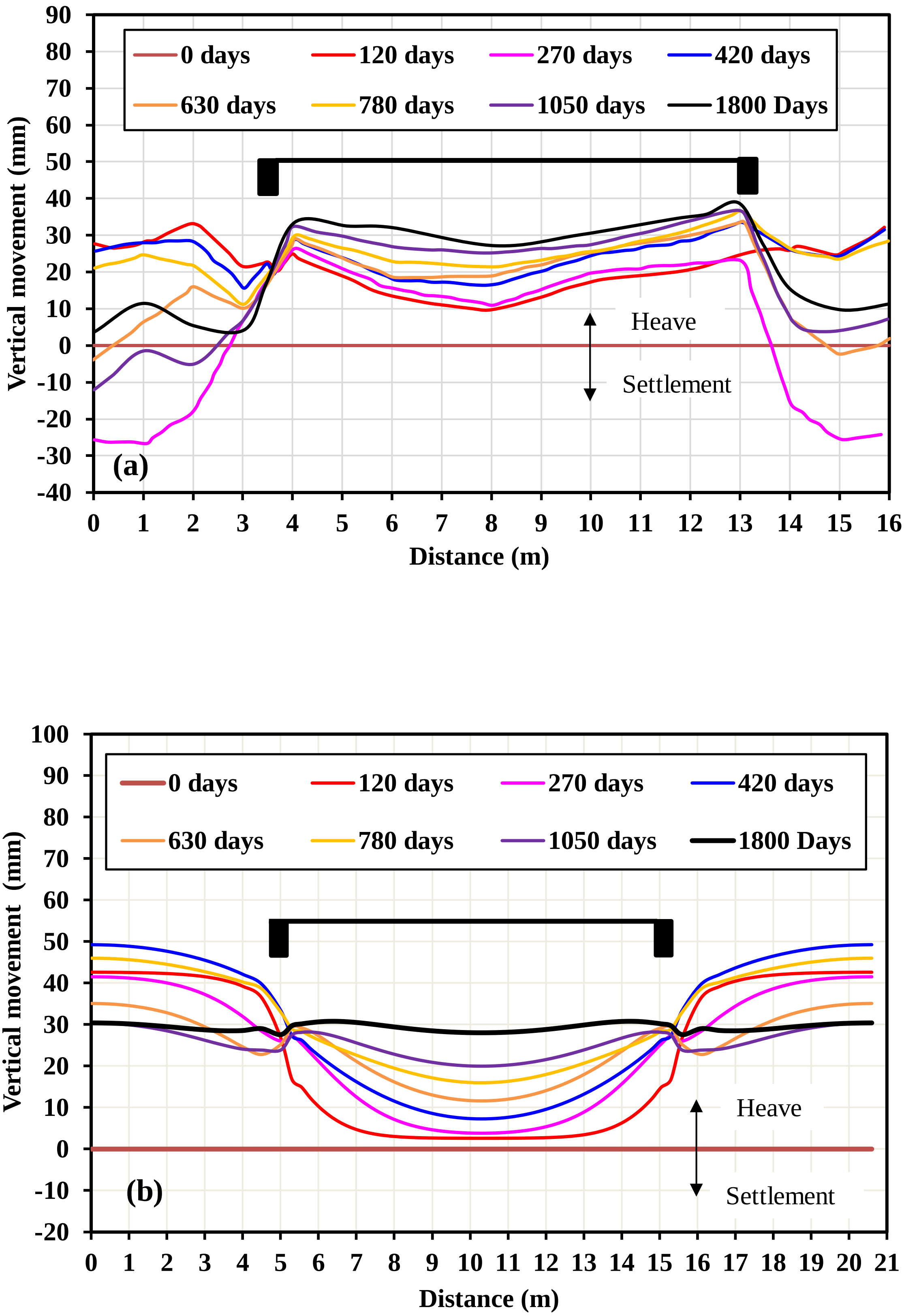

0 days
120 days
270 days
420 days
630 days
780 days
1050 days
1800 Days
Heave
Settlement
(a)
Vertical movement (mm)
Distance (m)
0 days
120 days
270 days
420 days
630 days
780 days
1050 days
1800 Days
Heave
Settlement
(b)
Vertical movement (mm)
Distance (m)

Fig. 6

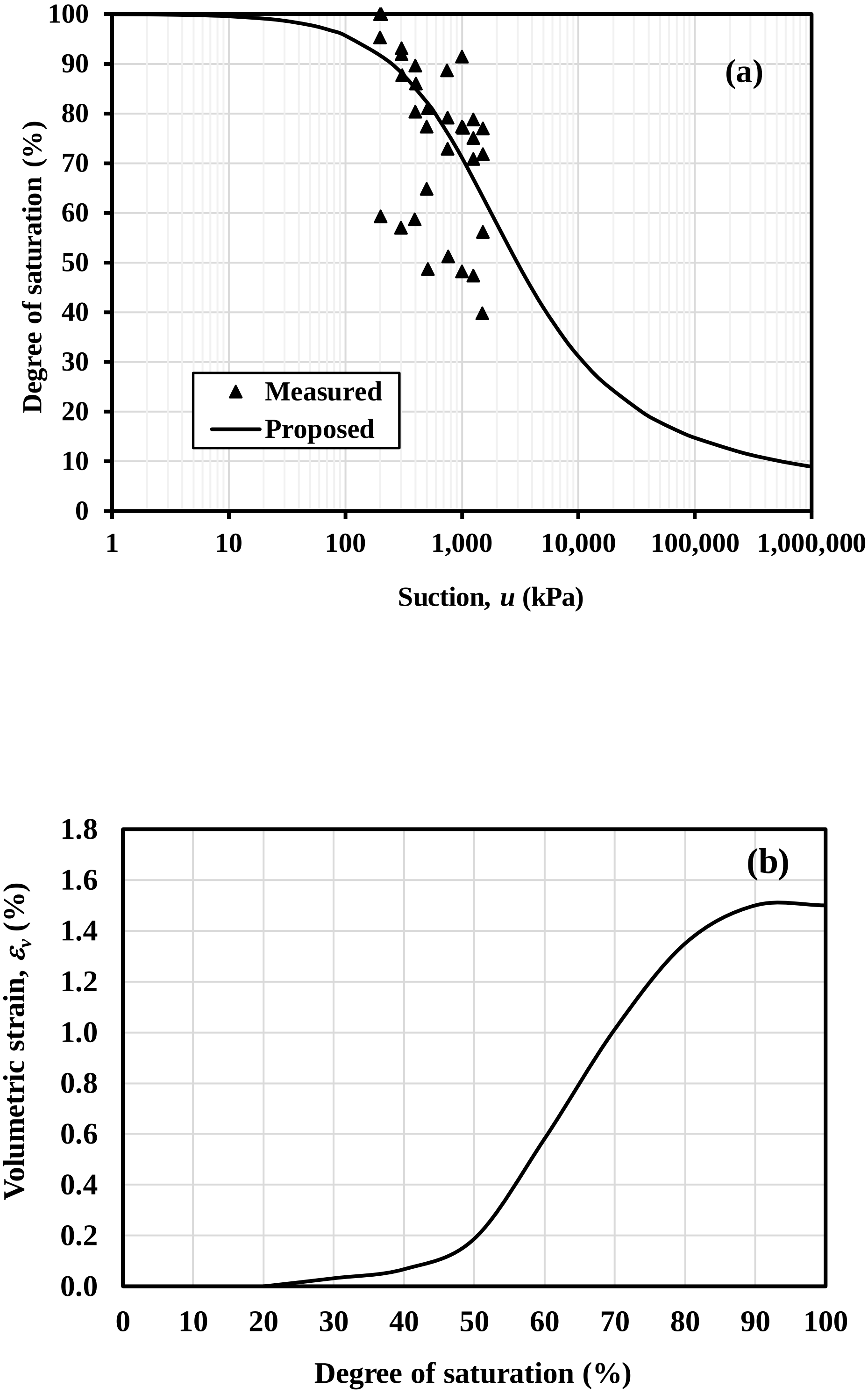

(a)
Degree of saturation (%)
100
90
80
70
60
50
40
30
20
10
0
1
10
100
1,000
10,000
100,000
1,000,000
Suction, u (kPa)
Measured
Proposed
(b)
Volumetric strain, ε_v (%)
1.8
1.6
1.4
1.2
1.0
0.8
0.6
0.4
0.2
0.0
0
10
20
30
40
50
60
70
80
90
100
Degree of saturation (%)

Fig. 7

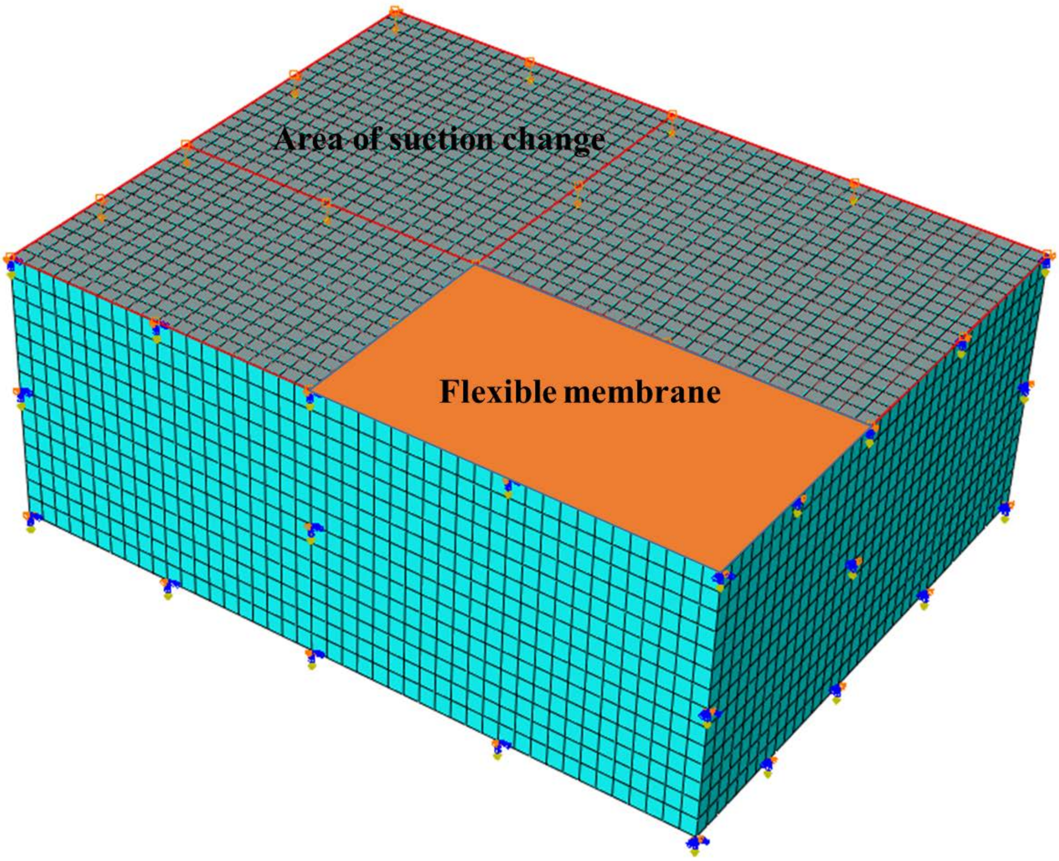

Fig. 8

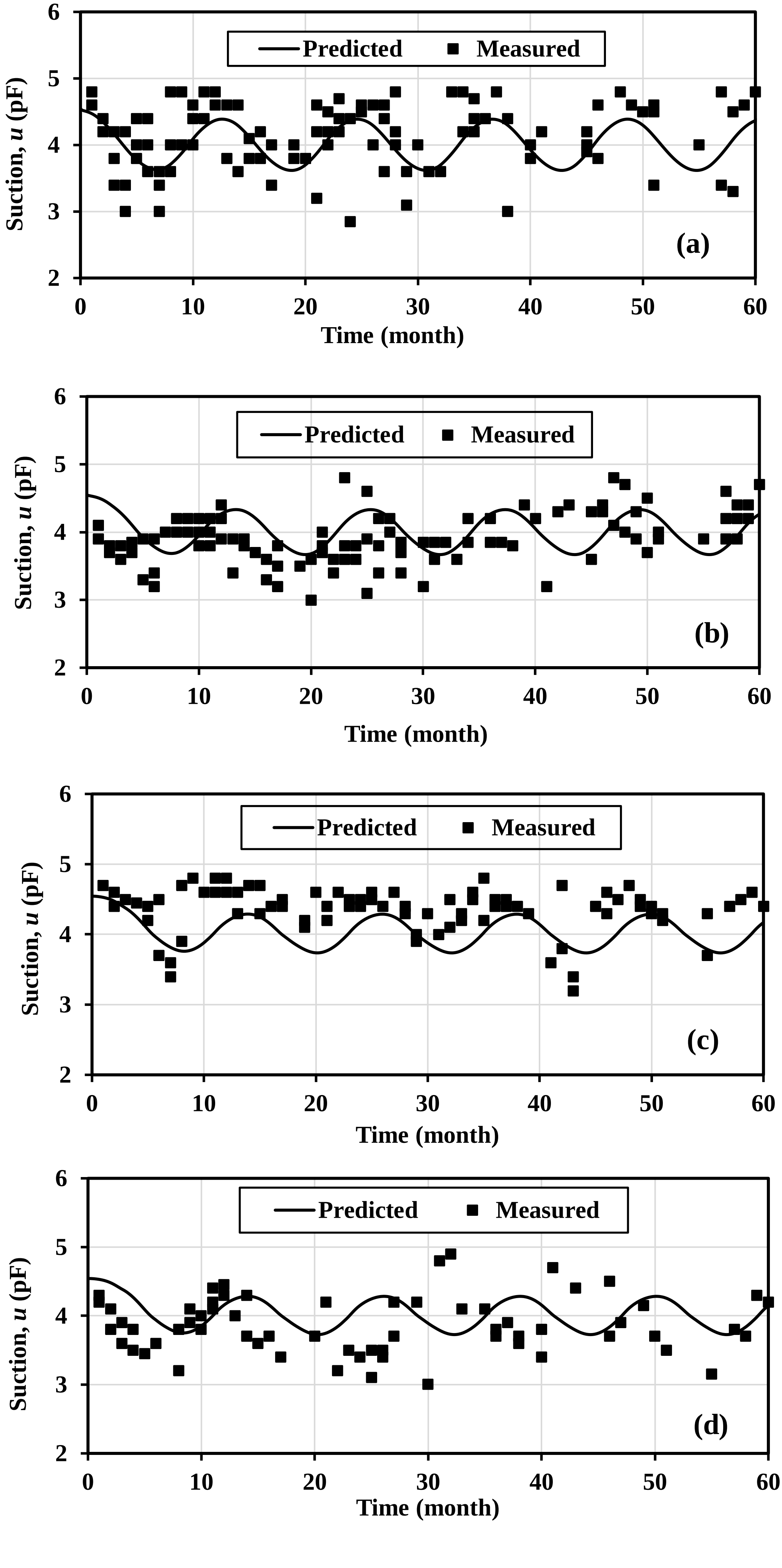

Fig. 9

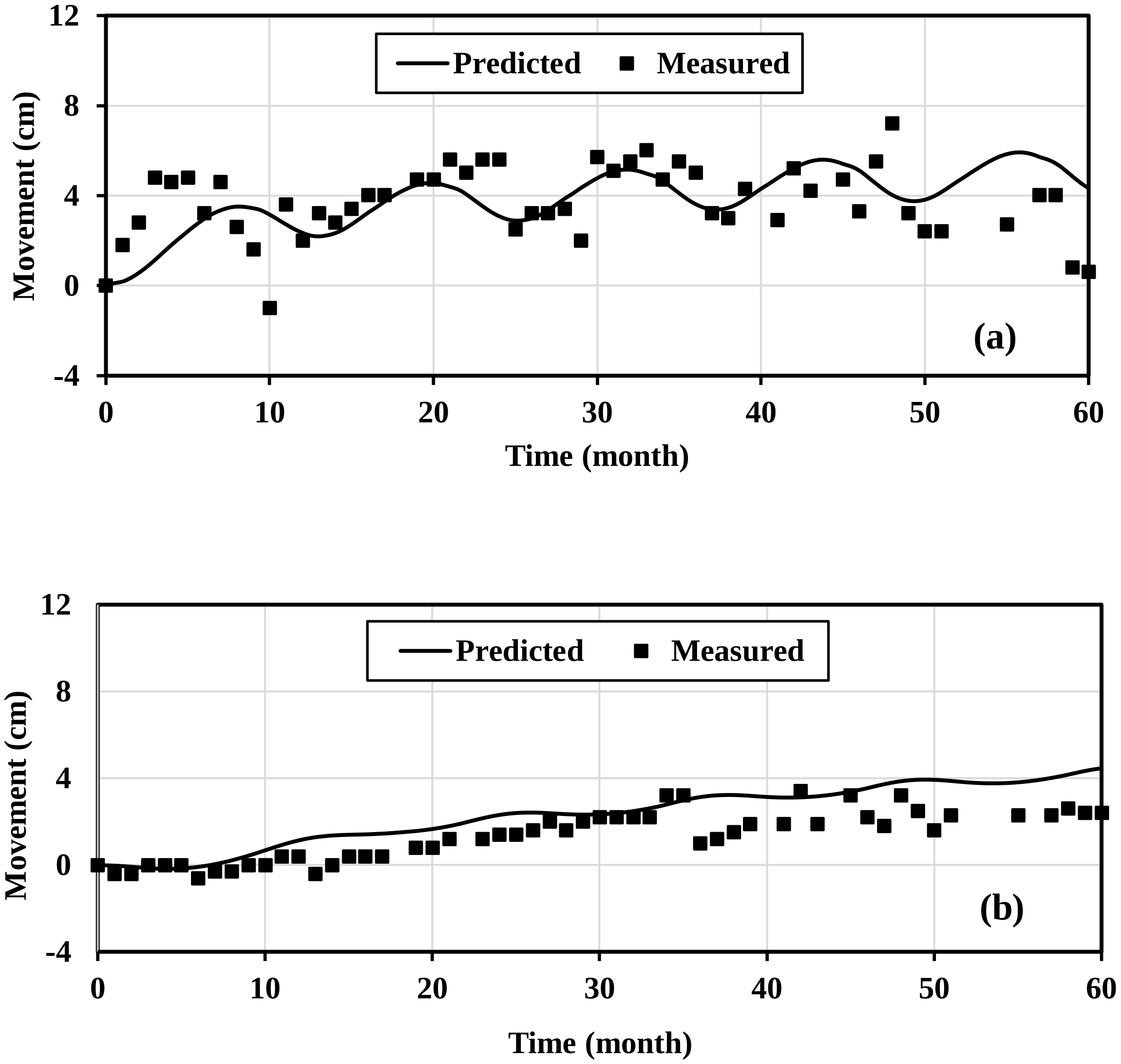

Predicted
Measured
(a)
Movement (cm)
Time (month)
(b)
Movement (cm)
Time (month)

Fig. 10

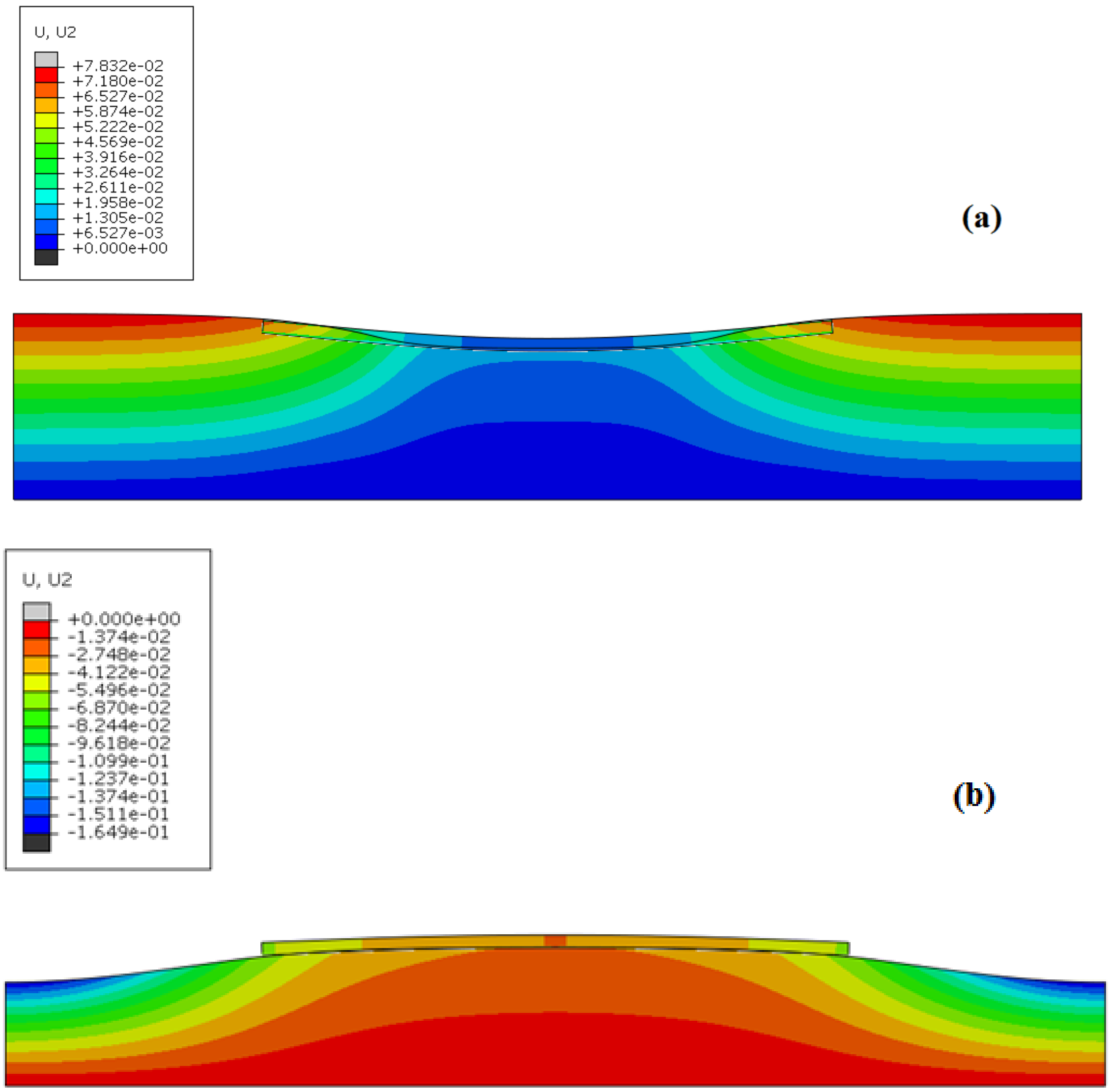
U, U2
+7.832e-02
+7.180e-02
+6.527e-02
+5.874e-02
+5.222e-02
+4.569e-02
+3.916e-02
+3.264e-02
+2.611e-02
+1.958e-02
+1.305e-02
+6.527e-03
+0.000e+00
(a)
U, U2
+0.000e+00
-1.374e-02
-2.748e-02
-4.122e-02
-5.496e-02
-6.870e-02
-8.244e-02
-9.618e-02
-1.099e-01
-1.237e-01
-1.374e-01
-1.511e-01
-1.649e-01
(b)

Fig. 11

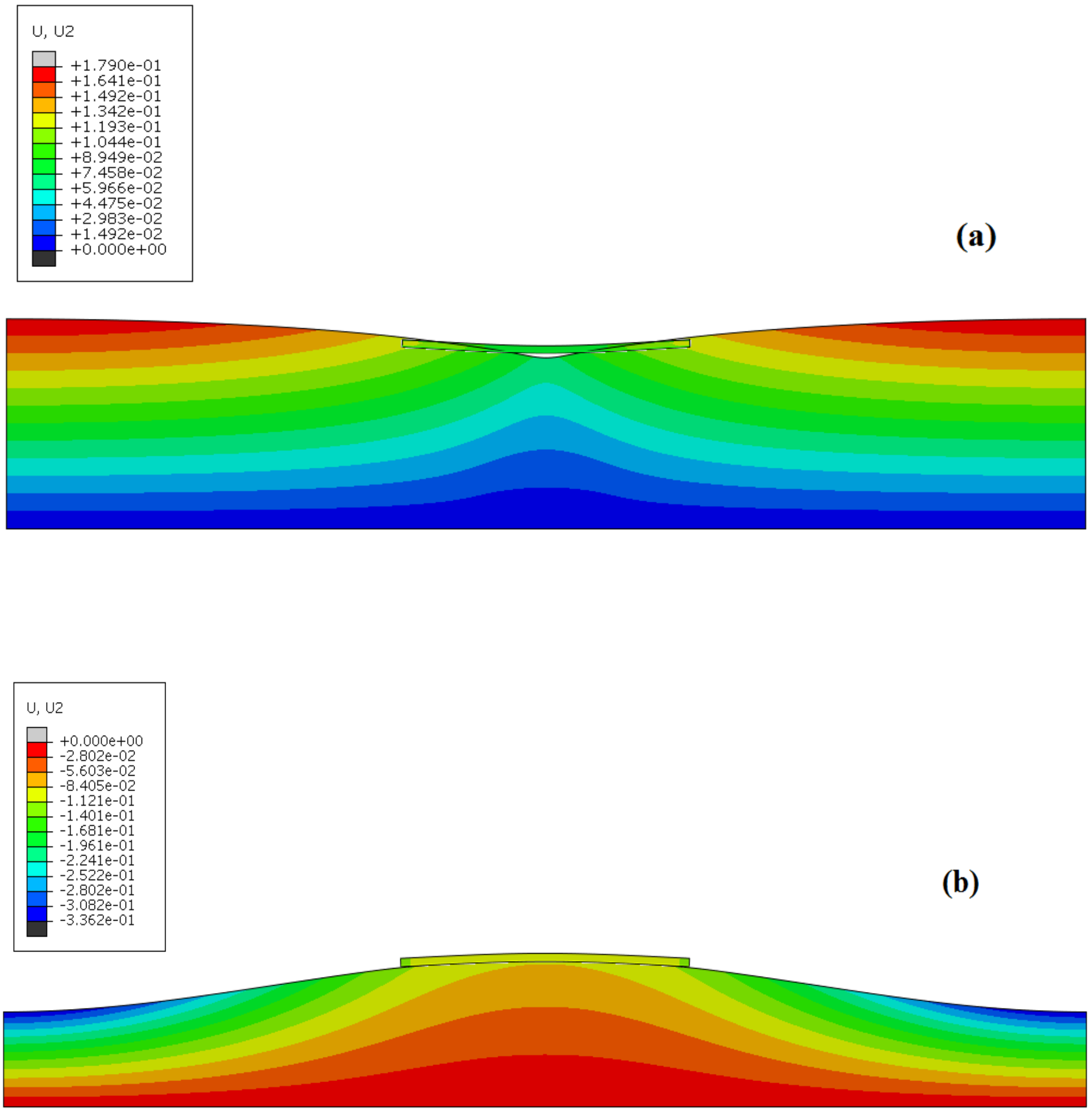
U, U2
+1.790e-01
+1.641e-01
+1.492e-01
+1.342e-01
+1.193e-01
+1.044e-01
+8.949e-02
+7.458e-02
+5.966e-02
+4.475e-02
+2.983e-02
+1.492e-02
+0.000e+00
(a)
U, U2
+0.000e+00
-2.802e-02
-5.603e-02
-8.405e-02
-1.121e-01
-1.401e-01
-1.681e-01
-1.961e-01
-2.241e-01
-2.522e-01
-2.802e-01
-3.082e-01
-3.362e-01
(b)

Fig. 12

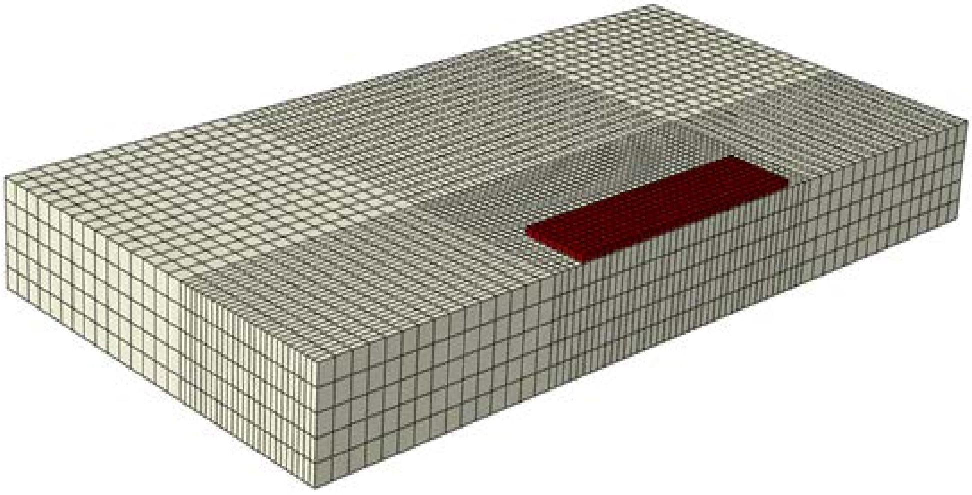

Fig. 13

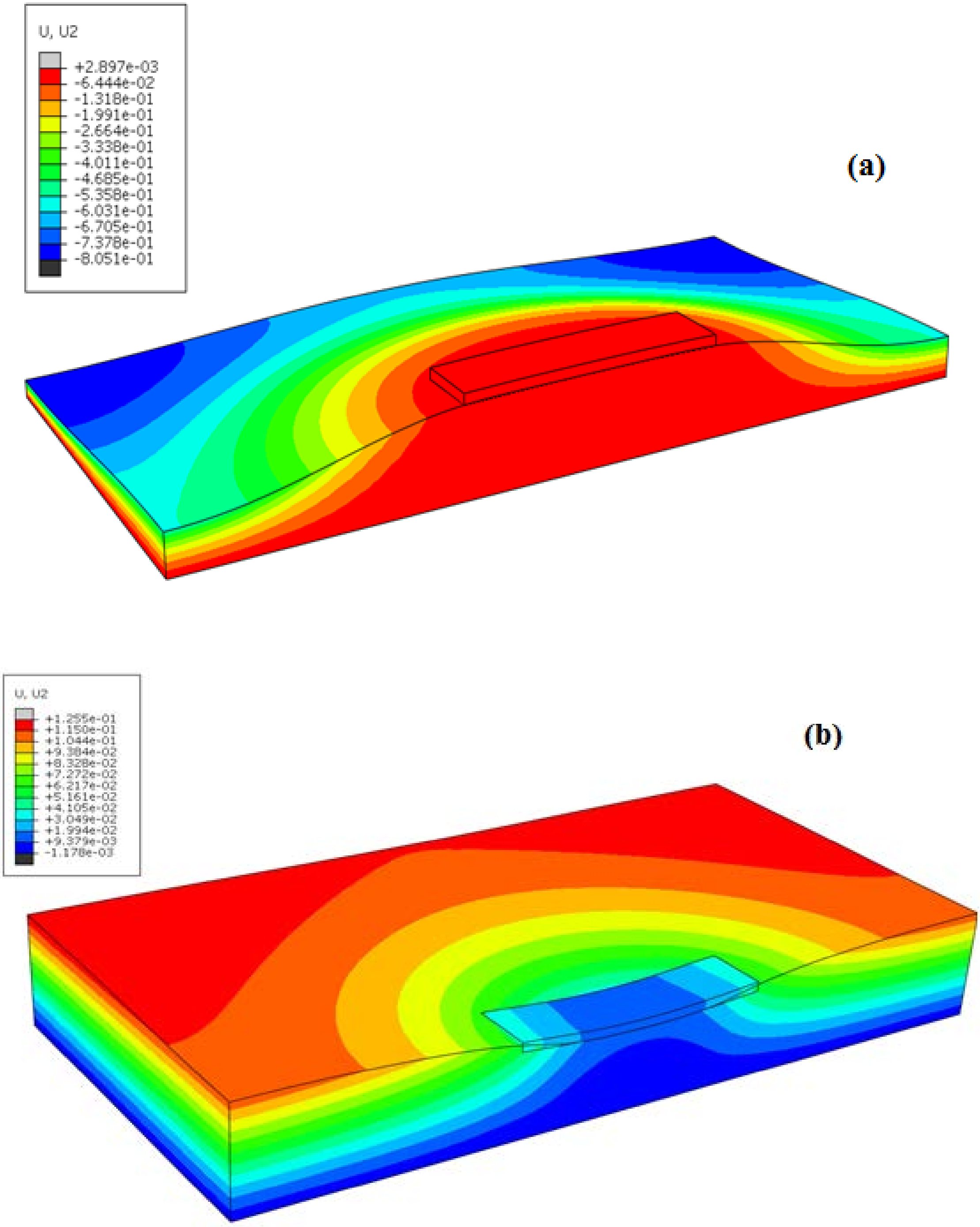
U, U2
+2.897e-03
-6.444e-02
-1.318e-01
-1.991e-01
-2.664e-01
-3.338e-01
-4.011e-01
-4.685e-01
-5.358e-01
-6.031e-01
-6.705e-01
-7.378e-01
-8.051e-01
(a)
U, U2
+1.255e-01
+1.150e-01
+1.044e-01
+9.384e-02
+8.328e-02
+7.272e-02
+6.217e-02
+5.161e-02
+4.105e-02
+3.049e-02
+1.994e-02
+9.379e-03
-1.178e-03
(b)

Fig. 14

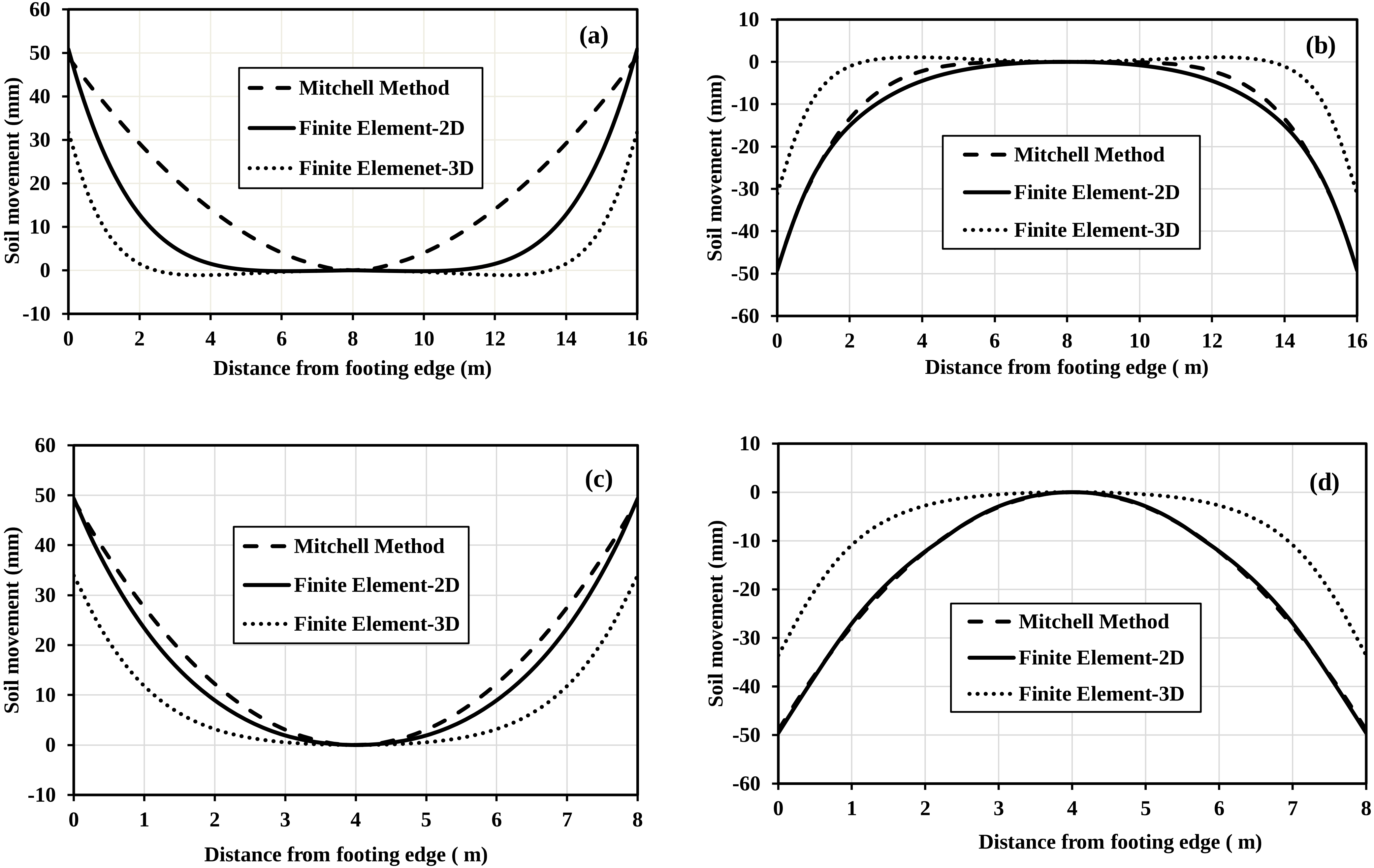
(a)
Mitchell Method
Finite Element-2D
Finite Elemenet-3D
Soil movement (mm)
Distance from footing edge (m)
(b)
Mitchell Method
Finite Element-2D
Finite Element-3D
Soil movement (mm)
Distance from footing edge (m)
(c)
Mitchell Method
Finite Element-2D
Finite Element-3D
Soil movement (mm)
Distance from footing edge (m)
(d)
Mitchell Method
Finite Element-2D
Finite Element-3D
Soil movement (mm)
Distance from footing edge (m)

Fig. 15

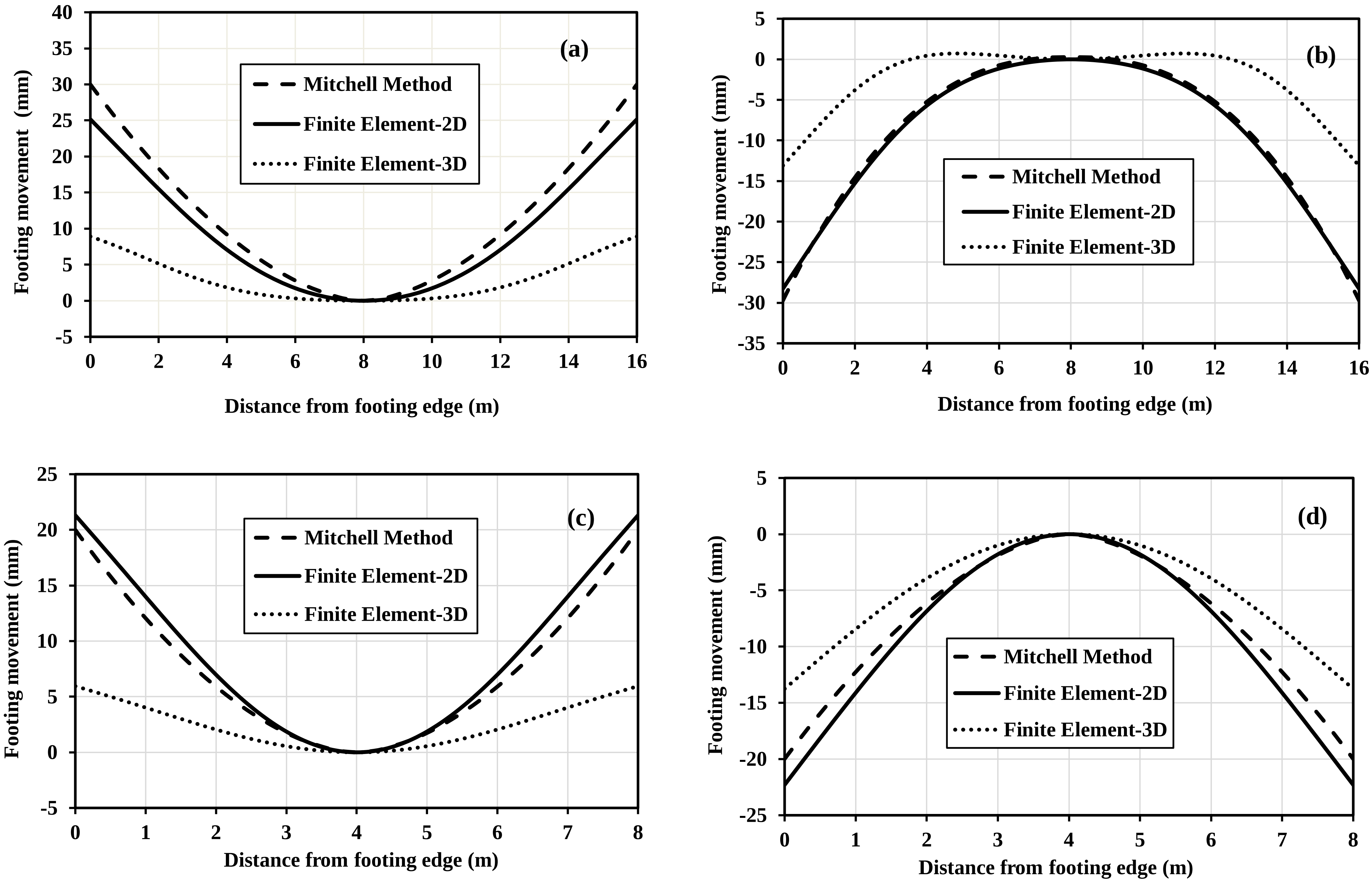
(a)
Mitchell Method
Finite Element-2D
Finite Element-3D
Footing movement (mm)
Distance from footing edge (m)
(b)
Mitchell Method
Finite Element-2D
Finite Element-3D
Footing movement (mm)
Distance from footing edge (m)
(c)
Mitchell Method
Finite Element-2D
Finite Element-3D
Footing movement (mm)
Distance from footing edge (m)
(d)
Mitchell Method
Finite Element-2D
Finite Element-3D
Footing movement (mm)
Distance from footing edge (m)

Fig. 16

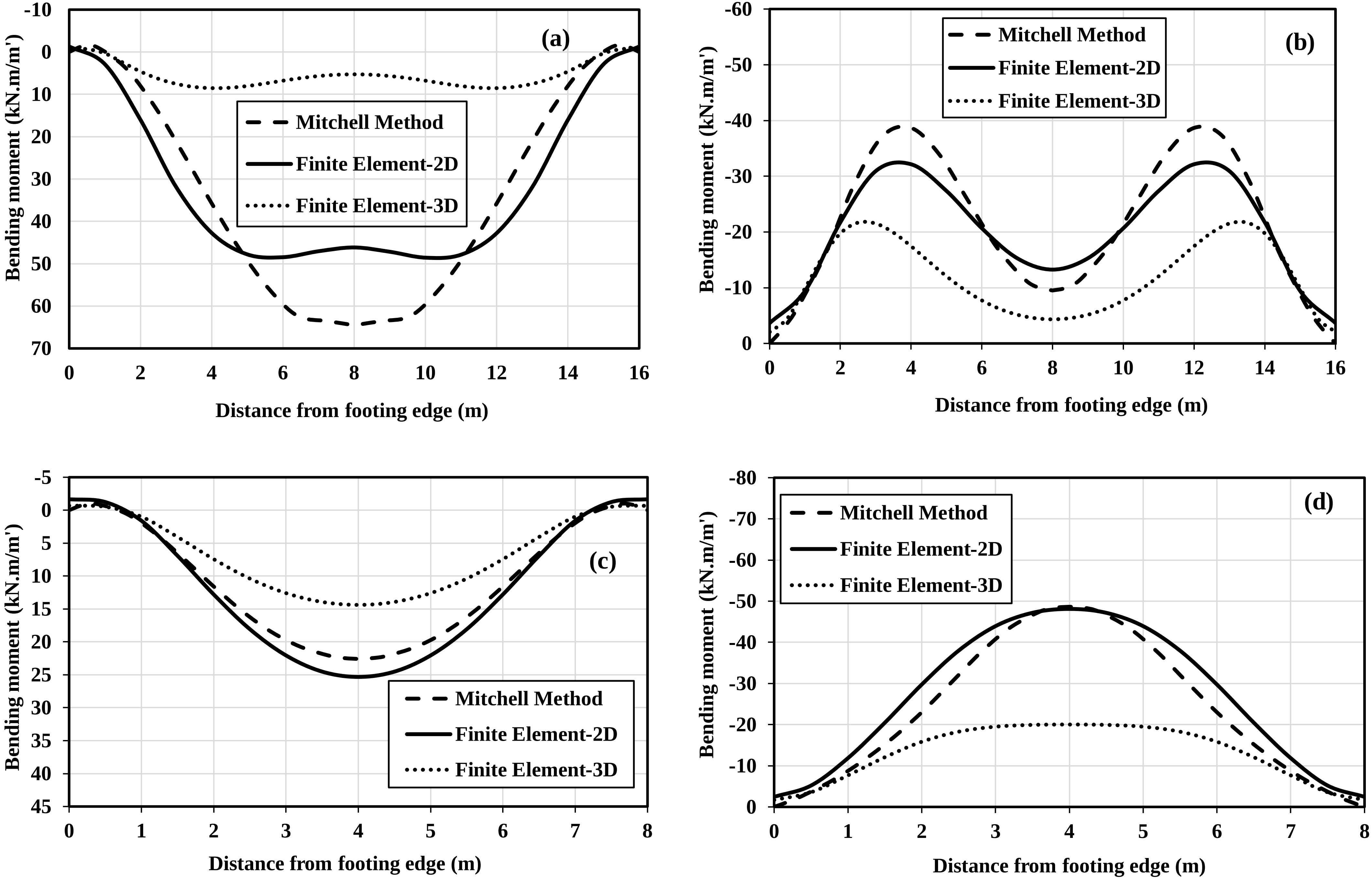

(a)
Mitchell Method
Finite Element-2D
Finite Element-3D
Bending moment (kN.m/m')
Distance from footing edge (m)
(b)
Mitchell Method
Finite Element-2D
Finite Element-3D
Bending moment (kN.m/m')
Distance from footing edge (m)
(c)
Mitchell Method
Finite Element-2D
Finite Element-3D
Bending moment (kN.m/m')
Distance from footing edge (m)
(d)
Mitchell Method
Finite Element-2D
Finite Element-3D
Bending moment (kN.m/m')
Distance from footing edge (m)

Fig. 17

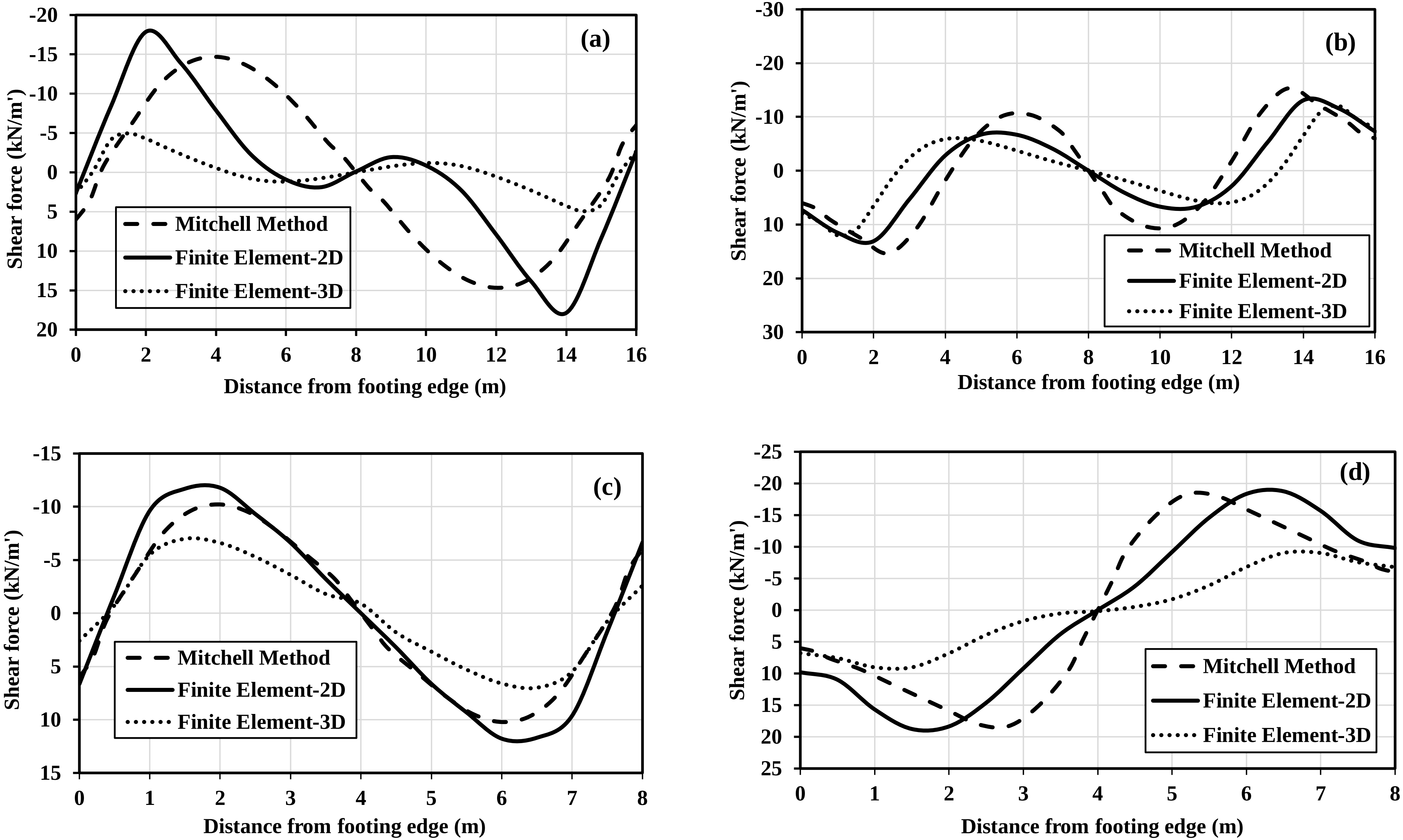

(a)
Shear force (kN/m')
Distance from footing edge (m)
Mitchell Method
Finite Element-2D
Finite Element-3D
(b)
Shear force (kN/m')
Distance from footing edge (m)
Mitchell Method
Finite Element-2D
Finite Element-3D
(c)
Shear force (kN/m')
Distance from footing edge (m)
Mitchell Method
Finite Element-2D
Finite Element-3D
(d)
Shear force (kN/m')
Distance from footing edge (m)
Mitchell Method
Finite Element-2D
Finite Element-3D

Fig. 18

Table 1

Heave scenario	Footing equivalent rectangular thickness (m)	
	Long span	Short span
Edge lift	0.35	0.175
Edge drop	0.27	0.22

Table 2

Material	Element type of FE mesh	Elastic modulous, *E* (MPa)	Poisson's ratio, v
Swelling Clay	C3D8P: An 8-node brick, trilinear displacement, trilinear pore pressure element	Following user subroutttine USDFLD (refer to Appendix A)	0.30
Slab Foundation	S4R: a 4-node doubly curved shell element	1.5 × 104	0.16